2014

An investigation into the use of the MOSkin detector for beam profile and output measurements in stereotactic and small field dosimetry

Dalia Hadaya
University of Wollongong

UNIVERSITY OF WOLLONGONG

Department of Engineering

An Investigation into the use of the MOSkin Detector for Beam Profile and Output Measurements in Stereotactic and Small Field Dosimetry

Dalia Hadaya

This thesis is presented as part of the requirement for the

Award of the Degree

Masters of Science –Research

From the

University of Wollongong

October 2014

Centre for Medical Radiation Physics

ABSTRACT

Stereotactic radiation therapy or radiosurgery involves the delivery of a radiation dose, using small radiation beams to treat tumours or lesions, typically within the brain. To derive accurate beam models for stereotactic treatment planning, high spatial and dosimetric accuracy is required. The stereotactic beams are required to be characterised with regards to dosimetry. The MOSkin detector developed by the Centre of Medical Physics at the University of Wollongong was investigated to determine if it could be used for dose characterisation of stereotactic small field radiation beams.

The MOSkin was compared to the IBA Stereotactic field diode (SFD), a PTW 31014 PinPoint chamber and Gafchromic EBT3 film. The dose characteristics examined were beam profiles and output factors over stereotactic cone diameters of 5 mm to 45 mm.

The beam profiles for the smallest field diameters measured with the MOSkin were conducted in two orientations ‘edge on’ and ‘face on’. The change in orientation from ‘face on to ‘edge on’ reduced the sensitive volume visible to the beam central axis. The MOSkin in the edge on position had improved spatial resolution, demonstrated by the smaller penumbra width (80% - 20%) for all nominal field sizes measured.

When comparing all investigated dosimeters, the stereotactic field diode demonstrated the smallest penumbra width for all beam profile measurements. A broader penumbra was observed with the PinPoint chamber over all field sizes. The MOSkin in the face on position was consistently within ±0.03 mm for all field sizes with respect to the SFD. EBT3 film results showed a broader penumbra for the smaller field sizes, which was unexpected and requires further investigation. The

penumbral width was consistently larger for EBT3 film with respect to the MOSkin for nominal field sizes of 5 mm – 10 mm.

In analysis of the output factors, the values were compared to in-house calculated Monte Carlo data. EBT3 film was shown to correlate well with the Monte Carlo data in the smaller field sizes, possibly due to its near water equivalence. The MOSkin, when compared to EBT3 film was shown to exhibit an over response of 2.6% at the smallest nominal field size of 5 mm, which could be due to the over response from the silicon components within the MOSkin. The MOSkin however, was shown to under respond at larger fields, in comparison to the Monte Carlo values. The SFD over responded for all output factor values in comparison to the Monte Carlo. The PinPoint chamber was observed to under respond at field sizes less than 10 mm, with an under response of 10.7% with respect to the Monte Carlo value at the 5 mm cone diameter.

The results of this investigation showed that the PinPoint should not be used for beam profile characterisation for stereotactic small fields unless a correction factor is applied. Overall, the MOSkin could possibly be used as a dosimeter for beam profile measurements, especially in the ‘edge on’ orientation, however data may warrant comparison to SFD measurements to minimise error.

Overall, no dosimeter can be used singularly to determine output factors in small field sizes, and all except the EBT3 film require correction factors due to non-water equivalence. The PinPoint in addition, requires a correction factor due to its significant volume averaging, causing significant dose perturbation at the smaller fields. The possibility of using the average output factor over all dosimeter used in this investigation to determine an output factor for each respective nominal field size should be investigated further.

ACKNOWLEDGEMENTS

First and foremost I would like to acknowledge and give a huge thank you to my clinical supervisor, Dr. Stephanie Corde Tehei, who spent many weekends and long nights working with me at Prince of Wales to collect my data. I will forever be grateful for her support and guidance throughout this research project and without her, this work would never have been possible. I would also like to thank the other radiation oncology medical physics staff at Prince of Wales Hospital, especially Simon Downes for giving me initial guidance and advice and allowing me access to the facilities to undertake my research. His support, particularly in the beginning of the project was invaluable and his clinical knowledge in radiation oncology is exceptional.

I would also like to thank my supervisors Professor Anatoly Rosenfeld, Dr. Dean Cutajar and Dr Jeannie Wong for their advice, support and incredible knowledge on the MOSkin. I would like to thank Professor Anatoly for his patience in a student who went on to conduct research at her full time position and 'forgot' she had a masters project to continue.

A would like to give a special thank you to the entire medical physics staff, especially the radiation oncology team at The Canberra Hospital including Dr. Helen Gustafsson, Jonathan Lee and Naonori Hu for helping out a colleague who's specialisation was not in radiation oncology but in imaging. They had never ending patience in answering all of my stereotactic and small field dosimetry questions and proof reading my work even with their busy schedules. I would also like to thank Jason Tse and Dr. Donald McLean, who also supported me throughout the project and gave me invaluable advice. Donald also allowed me to halt research projects, which allowed me to finalise my thesis, which I am very thankful and relieved for.

Dr. Sean Geoghegan should also be thanked for giving me time from operational work to complete my thesis.

Last, but definitely not least - To my very special family, especially my partner, thank you for your never ending support throughout my studies and into my career – I could never have done it without you all.

TABLE OF CONTENTS

LIST OF FIGURES

LIST OF TABLES

1 INTRODUCTION

Stereotactic radiation treatment is a certain type of external beam radiation therapy, which is becoming increasingly common. Stereotactic therapy involves the use of small radiation beams to treat the tumour target with high geometric and dosimetric precision. There are a number of challenges that are present under small field conditions including the existence of lateral charged particle disequilibrium, partial geometry shielding of the primary photon source and detector volume averaging effects.

Uncertainties in small field measurements and calculations can lead to errors within the patient treatment plan, which may lead to complications. Accurate measurements of the dose characteristics, including output factors and beam profiles are required to ensure accurate radiation delivery.

The significance now being placed on the challenges of small field dosimetry is indicated by the amount of time given to the topic at a number of international conferences including the 2010 meeting of the American Association of Physicists in Medicine (AAPM) and the recent publication of a report by the UK's Institute of Physics and Engineering in Medicine (IPEM) *(IPEM Report 103).*

The Centre of Medical Physics (CMRP) at the University of Wollongong has developed a MOSFET dosimeter called the MOSkin. The applicability of the MOSkin as a dosimeter for use in stereotactic fields is its small sensitive volume and high resolution, which should demonstrate if the MOSkin is comparable or possibly advantageous relative to small field dosimeters already in use.

This study is aimed at investigating if the MOSkin demonstrates accurate measurement of dose characteristics - beam profile and output factors for stereotactic

fields. The dose characteristics of the MOSkin are compared to the IBA stereotactic field diode, the PTW – Freiburg PinPoint ion chamber and EBT3 film.

2 LITERATURE REVIEW

2.1 Radiation Therapy

Radiation therapy can be used to cure, control and/or relieve symptoms of cancer. Approximately 50% of cancer patients would benefit from having radiation therapy at some time during their illness and is a vital part of curing approximately 40% of all cured cancers *(RANZCR 2014).*

Radiation therapy uses ionising radiation to damage and ultimately destroy cells in its treatment of cancer. If radiation has sufficient energy to eject one or more orbital electrons from the atom or molecule, the process is called ionisation and the radiation is said to be ionising radiation (*Metcalfe et al 2003).* Ionising radiation can cause damage to DNA through direct and indirect interactions that may initiate a series of events that lead to chemical and biological damage of the cell that can be lethal. Radiation therapy exploits the repair and repopulation difference between tumour and normal cells as tumour cells are less likely to recover than normal cells after irradiation.

In the treatment of cancer through radiation therapy, the aim is to localise and maximise the radiation to the cancerous region and minimise normal cell damage and complications. This is achieved through external and internal beam radiation therapy. External beam treatments typically use photons or electrons to deliver the radiation dose to the tumour site *(Metcalfe et al 2003).* The damage to the cell is related to the amount of energy deposited in a certain mass of tissue, the absorbed dose. The absorbed dose is measured in Grays (1 Gy = 1 J/kg). The larger the amount of radiation absorbed by the tumour cells, the lower the probability of cell survival *(Hall et al 2006).*

There are a number of techniques used in external beam therapy to shape the dose distribution so that it conforms to the target, including intensity modulated radiation therapy (IMRT) *(Web 2002, Teh et al 1999),* volumetric modulated arc therapy (VMAT) *(Otto, K 2008)* and stereotactic radiation therapy/surgery *(Leksell.L 1983).* Small field dosimetry, such as those present in stereotactic radiation therapy/surgery, is the topic of this thesis and will be discussed and evaluated within the following chapters.

2.2 Stereotactic Radiation Treatment

2.2.1 Introduction

Standard treatment of tumours in external radiation therapy is most commonly done with a linear accelerator (*linac*). Within this thesis, only radiotherapy treatment conducted using a linac will be visited.

The typical electron energies required in clinical practice for external beam radiation therapy other than the treatment of superficial lesions/tumours are over one Mega electron voltage (MeV). The linac accelerates a high energy beam of electrons to very high speeds (up to 99% of the speed of light) that are directed on to a target material, typically Tungsten. X-rays are then emitted from the target in the form of *Bremsstrahlung* (braking radiation), which is a process where accelerated charged particles emit electromagnetic radiation due to the deceleration and projection change of the electron as it nears the nucleus of the target atom. As the electron loses energy, the energy is converted into a photon due the law of conservation of energy *(Bushberg et al. 2010).* It is these x-rays that are used to irradiate the patient, with the potential to kill the cancerous cells. The unfortunate aspect is that normal tissue is also irradiated and damaged in the process of any tumour treatment.

The definition of tumour and target volumes for radiation therapy is vital to its successful implementation. This requires the best possible characterisation of the location and extent of the tumour. There are three volumes in radiation therapy as defined by ICRU 62 *(1999).* The first is the location and degree of gross tumour, i.e. what can be seen, palpated or imaged; this is known as the gross target volume (GTV). The clinical target volume (CTV) increases the GTV to add microscopic spread of the disease in surrounding tissue and areas of clinical risk such as lymph node groups. The third volume, the planning target volume (PTV) contains the CTV, plus a margin to allow for uncertainties in planning or treatment delivery and organ movement. The PTV ensures that the radiotherapy dose is delivered to the CTV *(ICRU 62 1999).* The importance of defining an accurate PTV is exemplified within small field treatments such as stereotactic radiation therapy/surgery.

2.2.2 Stereotactic Radiation Therapy and Radiosurgery

The aim of radiotherapy is to deliver a large radiation dose to a target volume while minimising the dose to surrounding normal tissue. Stereotactic radiosurgery/therapy (SRS/SRT) is the use of radiation ablation using very precisely focused radiation beams in place of conventional surgical excision to remove or create fibrous tissue in small target volumes *(Wong 2011, Ruud 2009, Podgorsak 2005, Taylor 2011).* With the increased accuracy and precision of linacs, and the continual development and advancement in tumour localisation accuracy, the use of stereotactic radiation for treatment of small lesions has become more abundant *(Taylor et al 2011).* Traditionally, SRS is used to treat brain or spine tumour or other abnormalities in a single fraction. SRS has also moved into SRT, where stereotactic treatments are conducted over multiple fractions to treat tumours. SRT is used to treat tumours in various scenarios including tumours that have been defined as too large to treat in the

one fraction (as this would cause an unacceptable level of normal tissue toxicity) or tumours near critical structures.

In 1951, Lars Leksell coined the term *stereotactic radiosurgery* with the goal to develop a method for 'the non-invasive destruction of intracranial lesions that may be inaccessible or unsuitable for open surgery' *(Chine 2008).* The technical realisation of this principle allowed Leksell to develop the gamma knife in 1967. The gamma knife is dedicated to stereotactic radiosurgery, whilst a linac is not.

The equipment used to conduct SRT and SRS deliver radiation with a high precision. To be effective it also needs to be based on accurate delineation of targets via computed tomography (CT), magnetic resonance imaging (MRI) and angiography of the brain. These imaging systems are able to achieve 3D or 4D volume reconstructions, so that the tumour and surrounding structures can be visualised accurately. Technological improvements in medical imaging and computing have led to increased clinical adoption of stereotactic treatment and have broadened its scope in recent years. In 2004, 45% of clinics in the United States offered SRS treatment by an AAPM profile of radiation oncology departments (AAPM 2004). In 2014, at least 12 major hospitals in Australia offer SRS.

The stereotactic radiation treatment is advantageous as the beam can be confined very precisely to the lesion, minimising radio toxicity to normal tissue, thus achieving dose reduction, especially to critical structures *(Grebe 2001).* Due to the tight conformation of the radiation beam to the tumour location and the relative smaller sizes of the tumour, higher doses of radiation can be used relative to standard radiotherapy, consequently improving the probability of local tumour control. This can also be described as a relative increase in therapeutic ratio, which is the ratio of tumour control to normal tissue complications.

However, the tight margins around the CTV used in stereotactic radiation treatment also increases the complexity of the delivery. Due to the relatively high doses used and highly conformal dose profiles, set up or localisation errors in the order of a few millimetres can cause severe under dosing of the target and overdosing of adjacent organs at risk (OAR). SRS/SRT quality assurance (QA) is therefore increasingly important with very tight linac machine tolerances, i.e. radiation and mechanical isocentre coincidence, couch top and imaging system precision (*Tyler et al 2013, Rowshanfarzad et al 2011*) . Incorrect output factor and profile calibration of linacs has caused the incorrect treatment and overdose of patients in Florida (77 patients), Toulouse (145 patients) and Springfield (152 patients) *(Schofield 2012).*

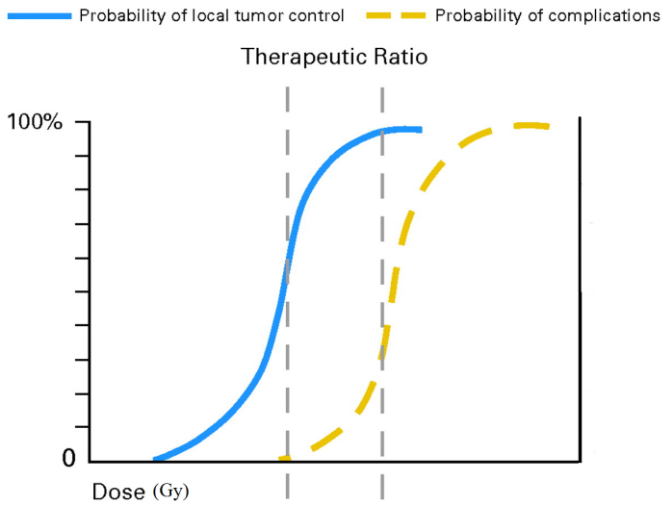

Figure 1. Therapeutic ratio: Increasing dose increases the probability of tumour cell death but also increases the probability of damage to healthy tissue

There are various machines available to conduct stereotactic radiation treatment including *conventional linac* based, the *Elekta Gamma Knife system*, the *Cyber knife stereotactic treatment unit* and various others. Only *linac* based stereotactic radiation treatments using circular collimators or *cones* will be discussed in this thesis. The cone is a device that collimates the radiation beam to a circular beam of a precise

diameter (figure 2). The cones are typically composed of lead surrounded by a shell of brass. Lead, due to its high density is an excellent attenuator of x-rays, and is used to attenuate most x-rays that are not forming the treatment radiation beam.

Figure 2. An example of stereotactic cones used to collimate the radiation beam

2.2.3 Challenges to stereotactic and small field dosimetry

A small treatment field can be considered to be a field size of less than 4 cm x 4 cm *(Taylor et al 2011)*. There are several dosimetric challenges encountered for small fields that are not seen in traditional radiation therapy treatment fields. These challenges include lateral charged particle disequilibrium (*Seuntjens 2011, Attix 1986*), partial blocking of the beam source giving rise to pronounced and overlapping penumbra (*IPEM report 103)* and the lack of availability of small detectors that are of sizes smaller than the field dimensions *(Das et al 2008)*

Lateral Charged Particle Disequilibrium

Electronic equilibrium is a phenomenon associated with the range of secondary particles and hence dependent on the beam energy and the composition, particularly

the density, of the medium *(Aspradakis et al 2010).* The condition for charged particle equilibrium is that for each particle that enters a volume *V* of mass *M,* an identical particle leaves the volume. When this requirement breaks down, electron disequilibrium occurs. Electron disequilibrium and its effect on dosimetry is explained below.

At mega electron voltage (MeV) energies, the electrons produced have a considerable range that gets prolonged in a low density medium. As derived by Li. X. A et al (1995), at 6 MV, a minimum beam radius of 1.3 g/cm^2 is required to achieve lateral electron equilibrium.

As the field size gets smaller, a limit is reached where the distance from the point of interaction to the closest field edge is smaller than the maximum range of the scattered secondary electrons *(Wuerfel 2013).* As a result, $R_{in} \neq R_{out}$ and lateral charged particle disequilibrium (LED) occurs. With small field sizes, this effect is significant enough to cause a total lower dose at the centre of the radiation field and a spreading of the penumbra.

a) b)

Figure 3, Charged particle equilibrium exists at the point of measurement in a) whereas non equilibrium conditions are seen in b) where the point of measurement is at the edge of a sharp dose gradient, affecting both the shape of the transverse beam profile and the absorbed dose.

Reference dose calibrations are performed according to IAEA report TRS 398 or AAPM Task group 51 in a well-defined beam geometry commonly using an

ionisation chamber as the reference chamber that is directly calibrated from a standards laboratory or cross calibrated against one. Dose measurements with ionisation chambers rely on the assumptions described in the Bragg-Gray cavity theory. The Bragg Gray cavity is a cavity (detector), which is so small that, when inserted into a medium, it does not disturb the fluence of charged particles existing in the medium. If charged particle equilibrium (CPE) exists, the ionisation produced within the gas filled cavity inside the medium is proportional to the energy absorbed in the surrounding medium *(Khan 2003).* As the field size decreases, electron spectral variations occur relative to the reference field, which causes an uncertainty of the dose in the small field compared to the calibration field is uncertain as the conditions for Bragg-Gray cavity theory break down *(Das et al 2008).*

Partial Volume effects

To measure the dose to a volume accurately, the dosimeter should be uniformly irradiated. Dose is measured by a dosimeter via the averaging of the measured charge over the entire sensitive volume of the detector, where charge is directly proportional to the dose. Dosimetry of small fields and steep dose gradients can be affected if the sensitive volume is large in comparison to the field size. In a small radiation field, the sensitive volume of the dosimeter can approach the field size. The sensitive volume may now measure over the flat field of the profile and include a portion of the penumbra. As the total measured dose is taken as the average dose over the sensitive volume, the dose measured would be inaccurate and result in a reduced signal. For any field that has a sharp dose gradient (fall off), the effect of volume averaging causes a broadening of the dose profile.

This brings about the importance of a dosimeter with a sensitive volume that is of a size that minimises the volume averaging effect and as such, a dosimeter with high

spatial resolution. When measuring the output factor for a particular field size, it is meaningful only if the dose is uniform over the dimensions of the detector. If an unsuitably large dosimeter was to be used for measurement of output factors for SRS/SRT fields, there is the potential to overdose the target and surrounding tissue due to the underestimation of the output factor. This would also cause the input data into the treatment planning system to be incorrect leading to miscalculation of dose volume histograms (DVH) as well as tumour control and normal tissue complication probabilities (TCP and NTCP respectively) *(Taylor 2010)*. Consequently, this can have significant effect on treatment outcome.

Laub and Wong (2003) reported local discrepancies of 10% between calculated profiles and those measured with film in regions of steep dose gradients. The variation between the dose profiles were characterised as a function of the large volume of the original detector used to collect beam data at commissioning. Through the use of a smaller detector, the absolute difference was reduced to 2%.

Source Occlusion

The photon fluence generated by a linac is composed of primary and secondary components. The primary radiation beam originates directly from the target focal spot whereas the secondary radiation is produced from scattered photons. For the purpose of source occlusion, the scatter produced from the structures in the linac head is most important. Jaffray et al (1993) identified that secondary radiation can contribute up to 8% in a 6 MV beam. The target is not a point as such but a spread over an area and the exit profile size is determined by the full width half maximum (FWHM) of the source profile. As the field size decreases, with decreasing collimator settings, the secondary radiation or scattered radiation is blocked by the collimators and its significance in the absorbed dose measurement is reduced. As the

collimator size decreases and approaches the size of the FWHM of the source profile, the radiation beam originating directly from the target is also attenuated and blocked by the collimators. The output will then be lower than compared to field sizes at which the entire source can be viewed from the detectors field of view (FOV).

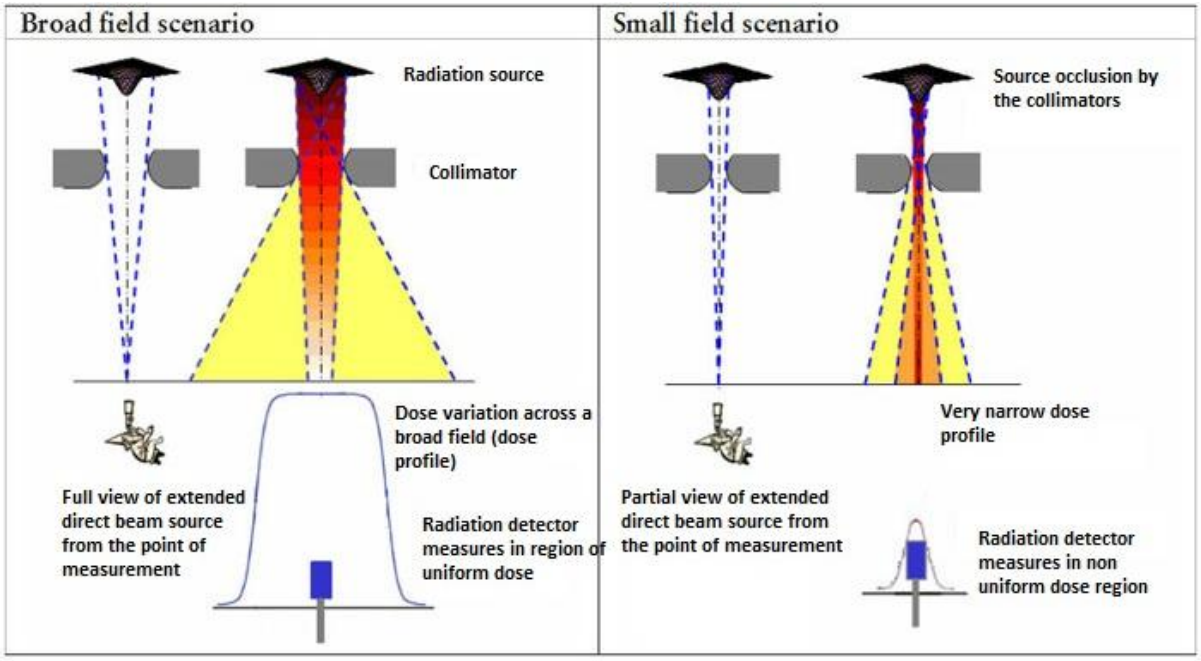

Figure 4. Broad field vs. small field (Aspradakis and Burne 2011©)

2.2.4 Ideal dosimeter requirements

Pappas et al (2008) states that the ideal detector for small field measurements should exhibit certain characteristics such as dose rate, energy and directional independence, tissue equivalency, high spatial resolution measurements, small sensitive volume, and not exhibit beam perturbation and positioning problems. The IPEM report 103 on small field MV photon dosimetry recommends the use of dosimeters with a small volume relative to the smallest field size under consideration that exhibit negligible perturbation.

Dose rate independence

The dose rate is defined as the dose per unit time. The dose rate may vary depending of detector position with respect to the beam and therefore should not affect the intrinsic response of the detector to ensure accuracy in dosimetry reading.

For dose rate independence, the response of the dosimetry system *M/Q* at two different dose rates $(dQ/dt)_1$ and $(dQ/dt)_2$ should remain constant where *M* is the reading measured by the dosimeter and *Q* is the dosimetric quantity being measured (i.e. charge) *(Podgorsak 2005)*. If the dosimeter is not dose rate independent, an appropriate correction factor is to be applied, which would have been determined at calibration. However the correction factor adds uncertainty of the dosimetry measurement.

Energy Independence

Treatment using small radiation fields are typically conducted using a 6 MV polychromatic photon beam on a linac and this photon spectrum might change when traversing medium. Accurate commissioning of the system before treatment is always required. Ideally, the radiation beam quality or energy should not affect the response of the dosimetry system. Typically, a dosimeter may have a flat energy response over a specified energy range; however a correction must be applied to the dosimetry measurement if the quality of the beam is out of this energy range.

Directional Independence

Small field radiation beam segments are used to treat the patient and are typically not conducted at the one angle. One example application of a dosimeter may be the determination of the total accumulated dose to the target region for a patient treatment plan. If the response of the detector varies with the angle of incidence of the radiation beam, the dosimeter will have some directional or angular dependence,

which may require correction. If a dosimeter is used in the same geometry as that which they were calibrated no correction would be required.

Tissue equivalence and beam perturbation

Ideally, the physical characteristics, such as the absorbing and scattering properties of the dosimeter to radiation should match that of water, which is used to simulate living tissue. If the detector does not have perfect tissue equivalence, it is seen to *perturb* the beam. Perturbation effects, as defined by Nahum (1996), are the departures from ideal large detector or Bragg-Gray cavity behaviour. It is necessary to correct perturbation effects for accurate dose determination in small field radiation therapy.

Small Volume

When identifying the characteristics of the dosimeter which would be most preferable for small field dosimetry, a small sensitive volume is always a requirement *(IPEM 103 2010, Khelashvili et al 2011, Duggan et al 1998 etc*). Johns and Darby *(1950)* proposed that dose profiles were artificially flattened in the penumbra region by detectors that were too large due to the volume averaging effect described earlier. For a minimisation of volume averaging in the penumbra region as well as for measurement of output factors for small fields, a very small sensitive volume is required. As the size of the sensitive volume decreases, the resolving power of the dosimeter in the ability to determine an accurate and true penumbra increases. The small sensitive volume also allows for a more accurate output measurement for the small field, which in turn permits more precise commissioning and dosimetry of small fields. Smaller detectors lead to smaller signal or charge collected, therefore high atomic number (Z) electrodes are introduced to increase the signal, however this leads to worse water equivalency.

2.3 Radiation Dosimeters

A radiation dosimeter is a device, instrument or system that measures or evaluates, either indirectly or directly, exposure, kerma, absorbed dose or equivalent dose, or their time derivatives *(Podgorsak 2005).* As discussed by Pappas *et al (2008)* and Bower *et al (1998)*, an ideal dosimeter for small field measurements should have the characteristics of:

1. Energy independence
2. Dose rate independence
3. Directional independence
4. Tissue equivalence/no beam perturbation effects
5. High spatial resolution/small sensitive volume

2.3.1 Ionisation Chamber

The ionisation chamber has been the work horse and standard radiation dosimeter for radiation therapy dosimetry due to its reproducibility, stability, linearity and portability *(TRS 398 2000).*

An ionisation chamber is a gas filled detector that is able to sense the ionisation created by radiation passing through the gas. The ionisation of the gas in the chamber results in a positive ion (+) and a free electron (-). The electric field created by the potential difference between the anode (positive) and cathode (negative) causes the charges to migrate and collect at the opposing charged electrode. Typically the ionisation chamber is designed with a conductive outer wall (outer electrode) and a central collecting electrode. The charge collected produces an electric current which is proportional to the absorbed dose in the chamber. This proportionality is determined at the time of calibration of the chamber *(Podgorsak 2005).*

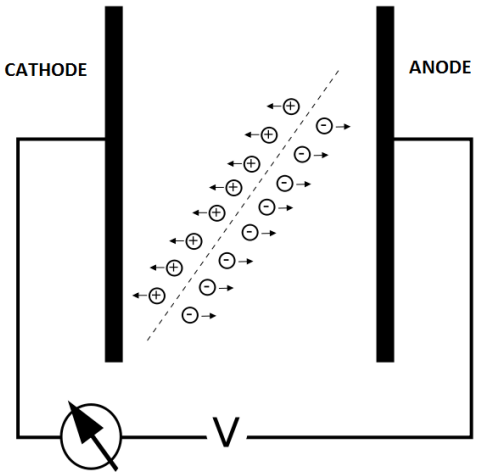

Figure 5. Effect of an electric field on charged particles

When performing measurements in small fields, it should not be assumed devices used for large fields perform optimally in small fields. This relates strongly to the ionisation chamber. For profile and penumbra measurements, a sensitive size ≤0.5mm is recommended to resolve narrow field penumbra without introducing significant volume averaging effects *(Pappas et al 2008)*. The most prominent disadvantage of the ionisation chamber is the size of the sensitive volume or cavity, which can affect the profiles in small or stereotactic beams (*Low et al 2003*). Air filled ionisation chambers generally have such size that the volume averaging is significant when measuring small fields where one dimension is smaller than 8 mm *(Aspradakis 2010)*. The farmer chamber, which is the most commonly used dosimeter for radiation therapy is often not suitable for small field dosimetry due to the volume averaging effect. Local discrepancies of more than 10% were found between calculated cross plane profiles and profiles measured with film in a study by Laub et al (2003).

The PTW-Freiburg Pinpoint ionisation chamber is specifically designed for small field dosimetry. There are three chamber models, 31014, 31015 and 31016 with sensitive volumes of 0.03 cm^3, 0.015 cm^3 and 0.016 cm^3 respectively. As Pappas et al (2008) identified even using the smaller sensitive volume PinPoint chamber, the

penumbra was artificially broadened over field sizes ranging from 7.5 mm – 30 mm. Other researchers have also reported that the PinPoint, due to its volume averaging effects, artificially broadens the penumbra *(Martens et al 2000, McKerracher et al 1999, Westermark et al 2000, Bucciolini et al 2003).*

The presence of a physical detector causes the charged particle fluence to differ from the fluence in water at the point of measurement in the absence of the detector. For ionisation chambers, this perturbation is caused by several factors including the presence of electronic and structural components, a detection material with a different atomic composition and density than water and a detector volume that is finite. The difference in atomic composition will cause the energy absorption in the detection material to differ from water *(Bouchard et al 2009).* The PinPoint chamber has an aluminium electrode, which influences the magnitude of perturbation caused by the chamber in the field as it over responds to low energy Compton scatter (Martens et al 2000).

Martens *et al* (2000) also identified that the PinPoint chamber is only suitable for fields greater than 2 cm though above 2 cm it is an excellent detector for output measurements. *PTW- Freidburg* (2013) have also recommended this chamber to be used for dosimetry measurements down to a 2 cm field size. The small volume thimble *IBA* chamber (0.01 cm^3 sensitive volume) specifically designed for stereotactic/IMRT dosimetry has a steel central electrode, which also causes perturbation effects in even greater extent compared to Aluminium.

Small liquid filled ionisation chambers are small in size, thus have a high resolution (*Aspradakis 2010*). These chambers also have a directionally independent response enabling measurements of profiles independent of the detector orientation *(Dasu et al 1998, Westermark et al 2000).* The PTW microLion detector is a commercial liquid

ionisation chamber, which may be a potential substitute to diodes; however a high voltage supply in the order of 1000 volts (V) is required for liquid ion chambers. The applicability of diodes to small field dosimetry is discussed in a later section.

2.3.2 Radiochromic Film

Radiochromic film consists of a base of thin plastic with a radiation sensitive dye coated uniformly on one or both sides (*Podgorsak 2005).* Once irradiated, the film takes on a blue hue or colouring. Irradiation triggers the formation of blue coloured polymers in the dye. The darkness of the colouring is non-linearly dependent on the amount of radiation absorbed by the dye. Using a densitometer or film scanner, the transmission of light through the exposed film can be measured and converted to absorbed dose through the use of calibration values for the specific film.

Radiochromic film has been used by several groups for small field dosimetry (*Ralston et al 2012, Gagnon et al 2011, Hsu et al 2011 and Hardcastle et al 2011*). The advantages of the use of Radiochromic film include the ability to self-develop once irradiated and that the effective atomic number is similar to soft tissue i.e. the film is approximately dosimetrically water equivalent. Radiochromic film is also grain less, allowing for a very high resolution when read out by conventional flat bed scanners (*Morales et al 2014).* This property makes it a very favourable choice for measurements in regions of high dose gradients such as the dose distributions in stereotactic fields (*Podgorsak 2005*).

Radiochromic film is virtually energy independent in the MeV region and only over responds by a few percent for energies of 25 keV or less *(Butson et al 2010).* One issue with the use of any film in dosimetry, including radiochromic film is that it is not a real time dosimeter. It also has uncertainties stemming from film orientation dependency, which will affect the accuracy of the measurement. Due to the way the

active components are aligned, variation in the film orientation within the film scanner may introduce errors. The effect originates from light scatter effects and is has the largest effect at the edges of the scanner bed. As a consequence, it is recommended that film scanning occurs at the central region of the scanner *(Richley et al 2010).*

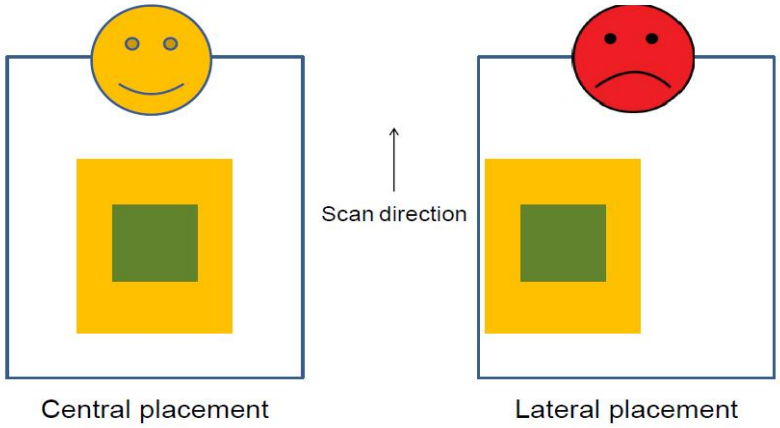

Fig 6: Lateral dependence of film position on the scanning area (Lewis 2012)

Another source of error involves the non uniform thickness across the film sheet, whereby different parts or regions of the film could have different dose responses *(Richley et al 2010)*. One must also consider the sensitivity of film to handling. Fingerprints as well as dust and lint can show up easily and radiochromic film can delaminate at cut edges.

EBT 3 film is the latest version in the Gafchromic EBT series. Gafchromic film (GaF) is a widely used type of radiochromic film in external beam radiation therapy. The composition and thickness of the sensitive layer are the same as the previous EBT 2 film *(Reinhardt et al 2012*); however EBT 3 film has a number of advantages over the earlier version. This includes a polyester substrate which prevents the formation of Newton rings and the use of a symmetrical structure for the different layers in the manufacturing of the film *(Morales et al 2014).* The film orientation

dependence is now eliminated with EBT3 film, which presents a major improvement for film handling (*Casanova et al 2013).*

2.3.3 Semiconductor Dosimeters

The advantage of the solid state detector is the much smaller and compact size of the detector relative to gas filled ionisation chambers as the solid densities are approximately 1000 times greater than that for gas *(Knoll 2000).* Devices employing semiconductors as the basic detection method became practically available in the early 1960s *(Knoll 2000).*

The basic definition of a semiconductor is a material with electrical properties that lie between those of conductors and insulators. At low temperature, semiconductors resist the flow of current, thus behaving like insulators. At high temperatures, however, semiconductors behave more like conductors, allowing current to flow.

Band structure in solids

When the discrete energy levels of individual atoms merge together solid bands of energies that contain a large number of closely spaced energy levels are formed *(Knoll 2000).* The lattice structure of crystalline materials establishes allowed energy bands for electrons in the solid. Electrons are confined to energy bands that may be separated by gaps or forbidden energy ranges. When defining the difference between conductors (metals), semiconductors and insulators, the energy bands of consideration are the valence and conduction band. The electrons of lower energy to those in the valence band are typically not considered as they have filled the lower shells and are tightly bound; they therefore do not contribute to the electrical conductivity of the material.

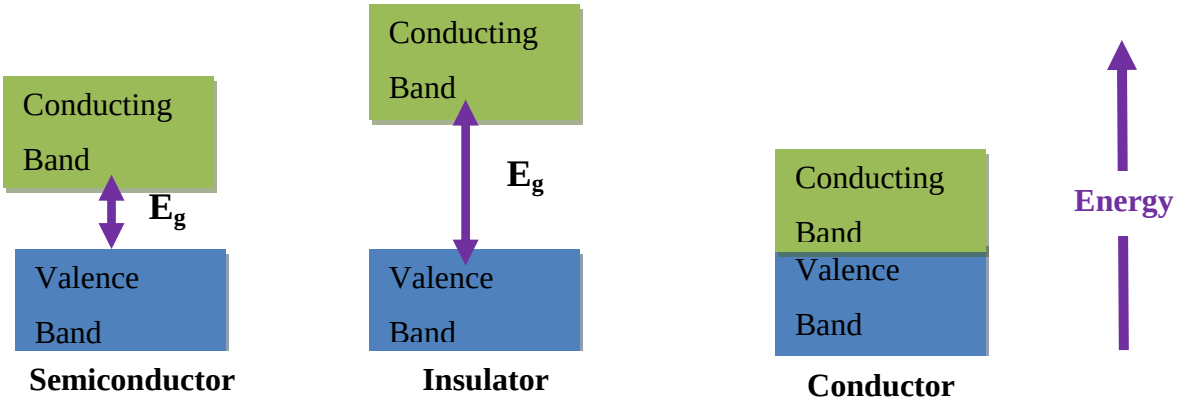

Figure 7. Energy bands of semiconductors, insulators and conductors (E_g) is the energy gap between the conduction and valence band

The valence band is located in the outer shell of the material and is bound to the lattice. The conduction band constitutes the electrons that are free to migrate and contribute to the conductivity of the material. The wider the energy gap (E_g) between the valence and conduction band, the larger the energy required to move an electron into the conduction band *(Knoll 2000).*

A conductor has no energy gap between the valence and conduction band, and electrons are free to migrate through the material. These 'free' electrons have the ability to move into the upper conduction band with a very small amount of energy i.e. the heat energy found at room temperature *(Knoll 2000).*

The semiconductor and insulator have energy gaps and the size of this energy gap classifies which type of material the solid is. For insulators, the outer electrons are very tightly bound and a large amount of energy is required for the electrons to cross the energy gap into the conduction band. In semiconductors, the energy gap is much smaller and at room temperature there will be electrical conductivity between the valence and conductive bands.

Effect of Impurities or Dopants

If an electron is to move to the conduction band, through the gain of thermal energy (*thermal excitation),* the electron leaves a vacancy or *hole* in the valence band, which represents positive charge. This is described as an electron-hole pair. In an *intrinsic* or *pure* semiconductor, the amount of holes in the valence band and electrons in the conduction band are equal and would be entirely caused by thermal excitation. If p and n represents the concentration of holes in the valence band and electrons in the conduction band, in a *pure* semiconductor *(Knoll 2000),*

$$n = p$$

In reality, no semiconductor is pure as they all contain some small inherent impurity or imperfection.

Impurities may be added intentionally to the semiconductor. Doping is the process of introducing impurity atoms, called dopants, into a semiconductor during their production. The presence of dopants in semiconductor materials increases the number of available charge carriers, either as holes or electrons, thus varying the materials electrical properties. There are two types of doping processes, n-doping and p-doping, which depend on the dopants and their location in the periodic table that are introduced into the semiconductor material *(Knoll 2000).*

Formation of N-type and P-type Semiconductor

Elements from group IV (four) in the periodic table such as silicon (Si) and germanium (Ge) can be considered as semiconductors. They have four electrons in their outer shell and have an affinity to form covalent bonds with group IV atoms in order to have eight electrons in the outer shell, thus filling the outer shell.

To form an n-type semiconductor, an atom from Group V can be used to dope Si lattice structure. A silicon atom is substituted with an atom from Group V (defined as

a donor impurity) and forms the covalent bonds as the substituted Si atom would. However, the dopant atom introduces a fifth electron, which does not form a bond, and is now only very lightly bound to the lattice and can occupy a position very near to the conduction band in the forbidden energy gap. It now only takes a relatively small amount of energy for this electron to move into the conduction band. Importantly, as this extra electron is not part of a 'lattice bond', a corresponding hole will not be formed when the electron moves into the conduction band.

An example of an n-type semiconductor is Si doped with Phosphorus (P), a Group V element.

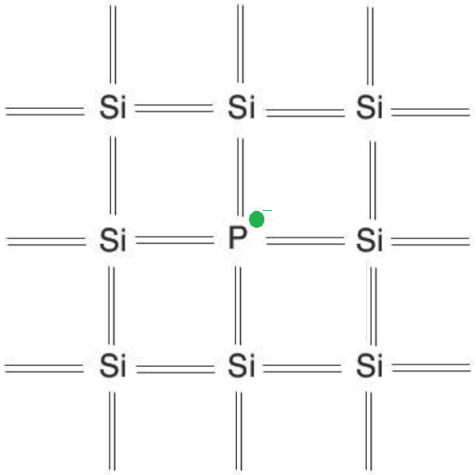

Figure 8. A diagram depicting the impact of a silicon crystal doped with phosphorus (a group V donor impurity)

P-type semiconductors are formed in the same way as n-type semiconductors, except the doping impurity is from Group III of the periodic table (an acceptor impurity) and thus has only 3 electrons in its outer shell. When the Si atom is substituted for the impurity, only three covalent bonds can be made, leaving one unpaired electron and a vacancy in the outer shell representing a hole. The electron that eventually fills this hole is less tightly bound then the other valence electrons and as with n-type doping can occupy a position in the forbidden energy gap, however, the energy position is much closer to the valence band relative to n-doping.

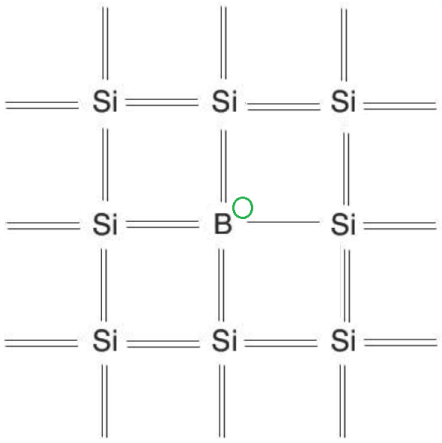

Figure 9. An example of a p-type semiconductor through the substitution of a Si atom with boron (B), an atom from group III.

2.3.3.1 Diamond detector

Diamond is the most stable form of carbon and has a wide band gap. The diamond can become a semiconductor through the introduction of impurities. The radiological properties of diamond are similar to tissue since the atomic number of carbon and that of tissue are very similar. Due to manufacturing difficulties, it is expensive; however it is well suited to small field dosimetry *(Das, I.J, 2008).* The PTW Freiburg diamond detector has a sensitive volume of less than 6 mm^3 and has been identified to provide high resolution and accurate small field profile measurements *(Pappas 2008).* Benmakhlouf et al (2014) also reported that the PTW diamond detector measures output factors within ± 0.8% of Monte Carlo simulated values.

2.3.3.2 Silicon diode

Silicon diodes are solid state detectors and are currently one of the smallest detectors available on the market (*Wuerfel 2013).* Due to the high signal to noise ratio, the sensitive volume of the diode can be made very small allowing for high spatial resolution. An example is the Scanditronix/IBA stereotactic field diode (SFD), with a sensitive volume of 0.017 mm^3. Small field diodes are commonly used in fields smaller than 30mm. Podgorsak (2005) and Aspradakis et al (2010) advise the use of the silicon diode in small fields used for stereotactic therapy and high dose gradients.

Knoll (2000) states that the reproducibility, stability, and linearity of the diode dose response are good.

One of the disadvantages of the silicon diode is the directional or angular dependence of the detector response *(Wuerfel 2013).* Wong and Laub (2003) identified a 3% dependence causing asymmetry in the low dose region of beam profiles at lateral distances from the central beam axis. Care should be taken with regards to the orientation of the diode with respect to the central beam axis. Other limitations include temperature and dose rate dependence *(Taylor et al 2013).* Diodes may also have an over response to low energy photons relative to water due to the higher density of silicon (ρ_{si} = 2.33 gcm^{-3}) *(Duggan et al 1998, Taylor et al 2013, Gagnon et al 2011, Scott et al 2012).* The dependencies of the diode need to be characterised before it is to be used for dosimetric purposes.

Dieterich and Sherouse (2011) identified that the IBA dosimetry Stereotactic field diode (SFD) shows a strong field size bias for output factors in comparison to other diodes including the Sun Nuclear EDGE detector, the PTW Freiburg TN60008 and PTW Freiburg TN60012. However, Brunet-Benkhoucha *et al* (2011) show that the SFD provides sharper penumbra when compared to the PTW microLion liquid chamber and IBA PFD Photon diode for small fields.

2.3.3.3 Metal Oxide Semiconductor Field Transistors (MOSFETs)

The use of a Metal Oxide Semiconductor Field Transistor (MOSFET) as a mean to measure cumulated dose was suggested as early as 1974 (*Holmes-Siedle 1974).* The structure of a MOSFET is a sandwich type device of a p or n-type silicon substrate separated from a gate electrode by an insulating silicon dioxide (SiO_2) layer (Figure 10). The gate controls the conductivity of the semiconductor material through the variation in magnitude of a bias voltage applied to the gate (V_g). The substrate can

only conduct current after a certain amount of voltage is applied to the gate, defined as the threshold voltage (V_{th}). The current originates from an electrode terminal known as the source (s) and flow through towards an electrode on the opposing end of the SiO_2 known as the drain (d) *(Kwan 2009)*.

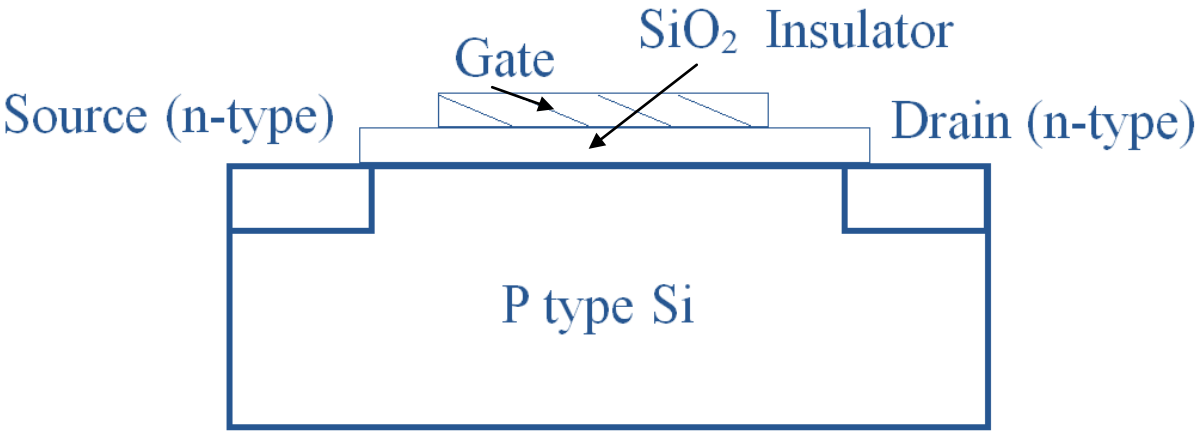

Figure 10. Schematic diagram of the structure of the MOSFET

When irradiated with ionising radiation, an electron in the valence band of the SiO_2 may have enough energy to move into the conduction band, forming a hole in the lattice. Consequently, electron - hole pairs are produced in the silicon dioxide. The placement of the bias voltage separates the electron hole pairs generated and decreases the probability of recombination. When the positive bias is applied to the gate, the electric field induced causes the electrons to move towards the gate whilst the holes move towards the silicon/silicon dioxide interface. The holes are captured in 'traps' located in the silicon dioxide layer and create a positive build up of charge. This positive charge sheet changes the current and a corresponding shift in the threshold voltage *(Rosenfeld 2002, Ramani 1997)*. The amount of radiation dose absorbed by the oxide is proportional to the change in the measured threshold voltage before and after irradiation, therefore the dose delivered to the MOSFET can be calculated *(Thomson-Nielsen, Peet et al. (1999), Podgorsak (2005))*.

Overall, the change in the threshold voltage for a MOSFET with a bias applied (*active mode)* can be described by:

$$\Delta V_{th} = 0.04 D t_{ox}^2 f$$

Where *D* is the absorbed dose, t_{ox}^2 is the thickness of the oxide and f is the fraction of generated holes that escape recombination. It has been shown that the sensitivity of the MOSFET is largely dependent on the oxide thickness *(Zahra 2009, Rosenfeld 2002).*

In the application of radiation therapy, the MOSFET has many advantages. It does not require energy correction at megavoltage beams, which is the energy range for radiation therapy stereotactic beams. The MOSFET has an extremely small sensitive volume, typically less than one micron *(Rosenfeld 2011),* which allows for a very high spatial resolution, it has the ability to store the accumulated dose as does thermoluminescent dosimeters (TLDs). It can be read out without deterioration of the dose information, which is not possible with TLDs. The sensitivity of the MOSFET can be increased by increasing the gate bias.

2.3.3.4 MOSFET device characteristics

Reproducibility

The reproducibility of a dosimeter refers to the ability to provide the same signal for consecutive measurements of equal dose. After irradiation, there is an exchange of charge between traps at the boundary between the Si and SiO_2. This is known as drift or a creep up effect, which can be several mV. It is important to wait between measurements to minimise the effect of drift. If a second measurement is conducted in close succession to the first measurement, the second injection of charge into the MOSFET chip can cause an amplification of the charge perturbation resulting in an

elevation of the apparent dose *(Ramani et al 1997).* If a wait period of one minute was used, Ramani et al (1997) detected that the creep up effect was negligible.

Energy Response

The probability of photoelectric absorption (τ) is proportional to

$$\tau \propto \frac{Z^n}{(hv)^3}$$

where the exponent *n* is energy dependent and varies between 3 and 5, identifying the high dependence of photoelectric absorption probability on the atomic number *Z (Knoll 2000).* The *Z* for Si is 14 and the effective *Z* for water is 7.4, therefore, for low energy photons (<100 keV), the photoelectric effect results in the emission of excess photo electrons from the MOSFET. This excess of photo electrons contribute to the dose measured, therefore the MOSFET over responds to low energy photons in comparison to water. Within the megavoltage (MV) photon energies, the MOSFET has no energy dependence, therefore no energy dependence correction is required. Ramaseshan et al (2004) also identified that the MOSFET had a uniform energy response observed in the therapy range between 4 and 18 MV.

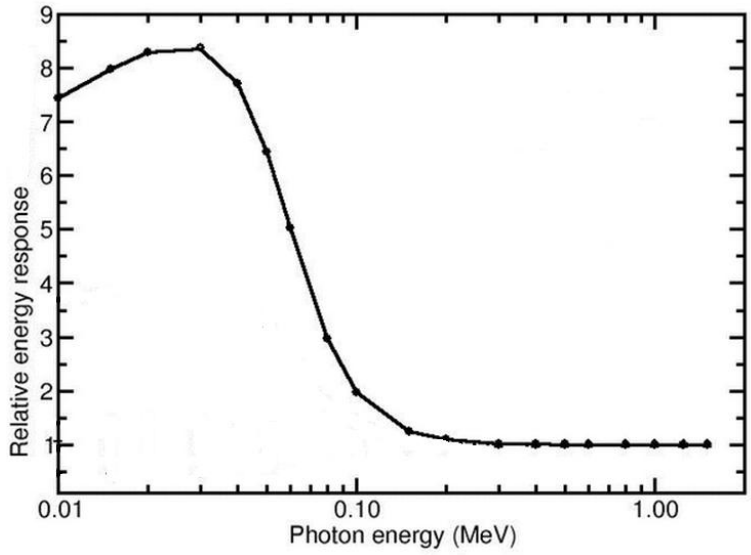

Figure 11. Energy response of silicon relative to water (Selvam et al 2010)

Temperature dependence

Cheung *et al* (2004) investigated the temperature effects on dosimetry over temperatures varying from 15 °C up to 40 °C using a MOSFET for radiotherapy treatments. The MOSFET radiation response remained stable over this temperature range, with a maximum variation of 1.5% (Figure 12). However it was noted that if there is a variation between the initial and final readout temperature, large differences in relative output were observed. When the reading temperature was kept constant, no difference in threshold voltage was seen. Consequently, to minimise error, if there is a large temperature change, the MOSFET may require a period of time to reach thermal equilibrium before measurement or can be readout with current corresponding to thermostable point on I-V characteristic[*Zara, 2009*] .

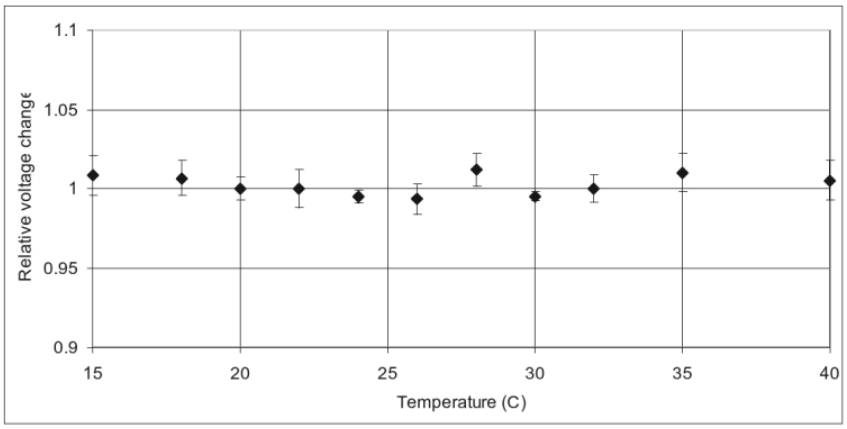

Figure 12. Relative threshold voltage change as a function of temperature when exposed to a dose of 100 cGy (Cheung et al 2004)

Dose rate response

Ramaseshan *et al* (2004) observed that no significant changes in response occurred to the MOSFET over a dose rate of 100 – 600 MU per minute. Qi, Z.Y. (2010) also identified that there was no significant dose rate dependence found for the MOSFET over a dose rate range from 100 – 400 MU per minute.

Linearity

Cheung *et al* (2004) measured the response of a MOSFET detector over the range 0 Gy to 30 Gy and found the response to be linear. However, if the MOSFET is used for a number of high dose readings, there is a point at which the dose to V_{th} relationship becomes non-linear. The non-linearity behaviour is a consequence of the build up of positive charge in the oxide traps, creating an electric field that counteracts the field produced by the bias voltage. The threshold voltage at which the non-linearity becomes considerable should be identified and one should ensure that the MOSFET dosimeter is replaced prior to the departure from linearity becoming significant, thus avoiding the potential underestimation of the radiation dose that might occur otherwise *(Benson et al 2004).*

2.3.3.5 The MOSkin Dosimeter

MOSFET dosimetry has many advantages due to the small size of the detectors sensitive volume, its memory of accumulated dose, the possibility of real time dosimetry/read out and ease of use. The increasing number of publications and studies on the MOSFET is suggestive of the importance of this dosimetry technique in radiation therapy and diagnostic radiology with more than 1500 publications within the last two years.

A new MOSFET called the MOSkin has been developed *(Rosenfeld et al 2001).* Typical MOSFET dosimeters utilize an epoxy resin that hermetically seals the electronics from moisture and protects the sensitive area from physical damage. The resin is placed on top of the sensor in a ‘bulb’ like shape. The base of the resin is shaped in an oval, which is aimed at maximising the uniformity of the epoxy thickness around the sensitive volume at all angles, and consequently, minimise angular dependence. The epoxy build up on the older style MOSFET detector was

also subject to variations in size leading to variation in the water equivalent detection depth *(Hayton 2011).*

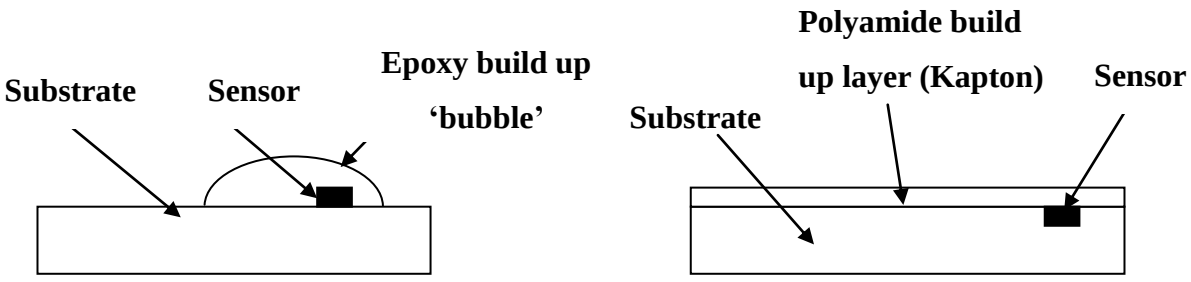

Figure 13. A schematic diagram of a) the traditional design of MOSFET detectors where the MOSFET chip sits on top of a substrate enclosed in a bubble of epoxy and b) the MOSkin

The MOSkin dosimeter does not contain an epoxy bubble layer to protect the sensor. The sensor or sensitive volume is located below the surface of the substrate the sensor is covered and hermetically sealed with a build-up layer of a water equivalent, flexible polyimide film (Kapton). The build-up layer can be manufactured to a highly reproducible specific thickness and therefore the build-up layer can be adjusted to suit the dosimetric application. Using the thin film build up layer rather than the epoxy bulb minimises the variability in the thickness of the build-up material between detectors. The MOSkin has been originally designed to conduct skin dosimetry *(Zahra 2009)* but due to its very small sensitive volume, will be assessed for its applicability in small field and stereotactic dosimetry.

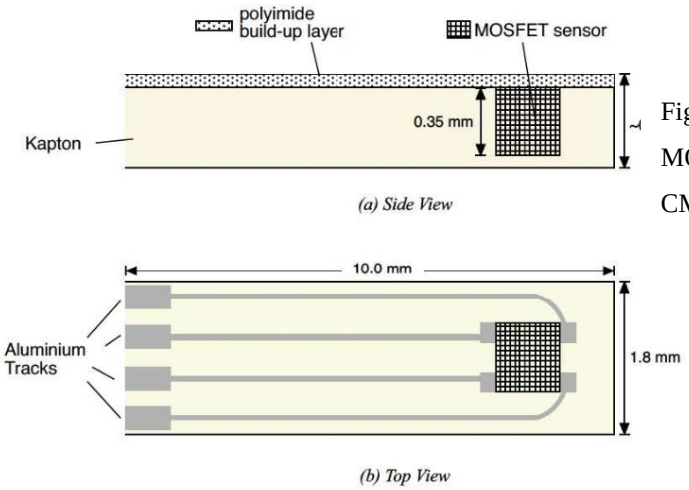

Figure 14. A schematic diagram of the MOSkin dosimeter designed by the CMRP (Kwan, 2009)

The MOSkin sensor has dimensions of 0.8 x 0.6 x 0.35 mm^3 (Figure 14). The gate oxide thickness is 0.55 μm, and the sensitive volume, defined by the volume of the gate oxide, is 4.8 x 10^{-6} mm^3 *(Gambarini et al 2013),* which allows for a high spatial resolution. The high spatial resolution of the MOSkin makes it a suitable dosimeter for use in steep dose gradients. The MOSkin dosimeter has been thoroughly characterised for a 6 MV beam with regards to temperature, sensitivity response, energy dependence and angular dependence *(Zahra 2009).* The MOSkin includes built in thermo stabilisation, which is independent of accumulated dose. Zahra identified that the MOSkin has low temperature instability of 0.2 mV/ $^{\circ}$C whilst the sensitivity response is 2.5 mV/cGy. The sensitivity was found to decline at a rate of 1.2% per 3 Gy while 'creep up' effects were not observed. It was also identified that the response of the MOSkin was dependent on energy, similar to other silicon devices. The response for 75 kV photons was shown to be 4.9 times higher than for 6 MV photons, however at MV energies, there is minimal energy dependence.

Due to the small sensitive volume, volume averaging effects should be minimal. Thus, the MOSkin should allow for accurate representation and characterisation of beam profiles used in small field radiation as well as the ability to determine the output for small fields such as those used in stereotactic radiation therapy. A read out system for the MOSkin has also been designed (*Rosenfeld et al 2001)*. The reader has the capability for five dual sensor MOSFET detectors to be read simultaneously.

3 METHOD AND MATERIALS

For this study, all irradiations were performed with a 6 MV photon beam on a Siemens Primus linear accelerator (Siemens Medical Solutions). An in-house set of stereotactic collimators (cones) and cone holder were fitted to the linac to collimate the beam. The collimating aperture of each cone is made with lead and is enclosed in an outer brass 3 mm casing which fixes the cone within the cone holder. The cones range from nominal field diameters of 5 - 45 mm defined at the isocentre (100 cm from the x-ray source). An IBA Wellhofer Blue Phantom three dimensional scanning water tank was used for all measurements other than film. The water tank was levelled before each session.

Due to the unavailability of a diamond detector, the detector was unable to be used within the experimentation in this thesis.

3.1 The MOSkin dosimetry System

The MOSkin detector has been described within the literature review above. See also Kwan (2009) and Zahra (2009) for more detailed information regarding the MOSkin dosimeter. The MOSkin was connected to an in house designed read out system. A gain of 15 V, placing the dosimeter in high sensitivity mode, was used for all measurements.

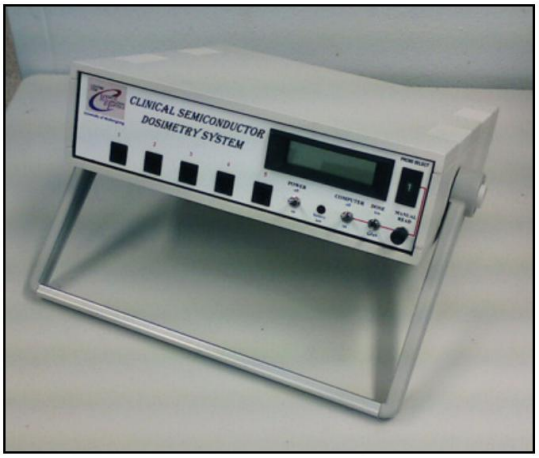

Figure 15: MOSkin reader

3.1.1 Phantom Design

As the MOSkin is not rigid, a phantom was designed to hold the MOSkin in the water phantom and minimise unaccounted movement. The phantom was made from Gammex solid water and specifically designed for the MOSkin. The phantom is in a cylindrical shape split into hemi cylinders. A groove was made in the solid water using the specific dimensions of the MOSkin to ensure that the top hemi cylinder would sit level with the other hemi cylinder.

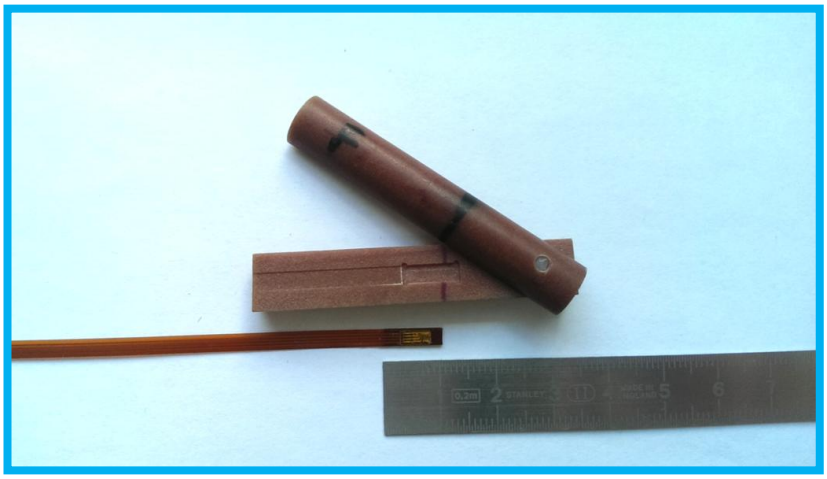

Figure 16. A MOSkin with the solid water phantom

3.1.2 MOSkin dosimeter selection

A selection of MOSkin detectors was made, and initial testing of threshold voltage and detectors reproducibility was performed. The dosimeters were attached to the read out system and the threshold voltage read 5 times. If the threshold voltage varied by more than 0.002 V over the readings, the MOSkin was rejected.

An experiment was conducted to ensure the reproducibility and stability of the MOSkin in water by placing the selected MOSkin detectors in water for 36 hours. The MOSkin were then read out every 5 hours to check if the threshold voltage had changed.

3.1.3 Priming and Calibration

Before any measurements were conducted, the linac was warmed up by delivering at least a 1000 monitor units (MU). The MOSkin was then primed.

The priming set up was:

Source to surface distance (SSD): 100 cm

Depth in water: 1.5 cm (D_{max} at 6MV)

Field size: 10 cm x 10 cm

Energy of beam: 6 MV

Dose: 200 MU or 2 Gy

The linac is calibrated at 1.5 cm depth in water on the beam central axis at 100 cm SSD in a 10 cm x 10 cm field for 1 MU to equal 1 cGy. Consequently, the MOSkin was calibrated in this setup. The dose was 100 cGy. The calibration factor in mV/cGy was determined before and at the end of each measuring session i.e. after each profile measurement. The MOSkin was manually read out 30 sec after the dose was delivered.

3.2 MOSkin Linearity of Dose Response

To assess the linearity of dose response of the MOSkin, the MOSkin was placed in the water phantom at 1.5 cm depth as described above. The response of the MOSkin was measured over the range 10 – 200 cGy.

3.3 Beam Profile Measurements

The MOSkin, PinPoint detector and stereotactic field diode beam profiles were obtained SSD 100 cm with the dosimeter at a depth of 1.5 cm in water. The secondary jaws on the linac were set to 4.6 cm x 4.6 cm and the cone applicator and selected collimation cone were mounted on the gantry. The location of maximum signal was determined by initially aligning the detector with the laser markers at 100 SSD then moving it down to 1.5 cm depth. To locate the position of maximum signal in the lateral direction each dosimeter was moved in increments of 0.5 mm in the inline plane. The dosimeter was moved out of field for the start of the profile. To minimise hysteresis effects, the profile was measured in one direction only. To determine the starting location of the profile for each detector, the equation shown below was used.

$$Starting\ point\ (cm) = \left(\frac{-(size\ of\ cone\ (cm))}{2}\right) - 0.3\ cm$$

3.3.1 MOSkin

Beam profile measurements for the MOSkin were conducted in two orientations: 'face on' and 'edge on' (figure 18).

Face on

The 'face on' beam profile measurements, the detector was placed facing the radiation beam (face up). The dose at each location (D_n) was normalised to $D_{max.}$ The step size was varied based on the value of $D_{n.}$

Step size:

- Tail region (normalised dose to max, Dn < 0.2) ➔ 0.1 cm
- Penumbra region ($0.2 < D_n < 0.8$) ➔ 0.03 or 0.05 cm
- Plateau region ($D_n > 0.8$) ➔ 0.05 or 0.1 cm

The smaller step size was required especially at the start of the penumbra region i.e. D_n ranging between the 0.9 and 0.7 regions of the beam profile to record the steep dose drop off with maximum accuracy and resolution. When conducting the 0.05 and 0.03 increments, due to the very small step size, the MOSkin was moved 0.1 - 0.5 cm from the original position and then moved back to the required position.

For each point on the profile measured, three measurements were taken manually and averaged to ensure reproducibility and minimise error. The standard deviation (S.D) and coefficient of variance (CoV) of the three measurements were also calculated.

The MU delivered for each region of the profile was guided by the uncertainty of the measurements via

$$Error(\%) = \frac{1mV}{\Delta V\ (mV)} \times 100$$

If the uncertainty was > 2%, the MU given was increased. As a general guide:

- Tail region : 300 MU
- Penumbra region: 100 MU
- Plateau region : 50 MU

The dose or change in threshold voltage (ΔV) was corrected for accordingly i.e. normalised to the MU delivered at the plateau.

Once the profile had been measured, the MOSkin was moved back to the location at which D_{max} had been identified and an additional reading was obtained at this point. This was to both check accuracy in dose and in the positional movement of the dosimeter in the water tank.

Once the MOSkin reached 20V, the MOSkin was not to be used due to the tail off of the dose response as discussed earlier. To minimise uncertainty, one MOSkin was used for each beam profile, which allowed for the threshold voltage to not near the 20 V in any measurement.

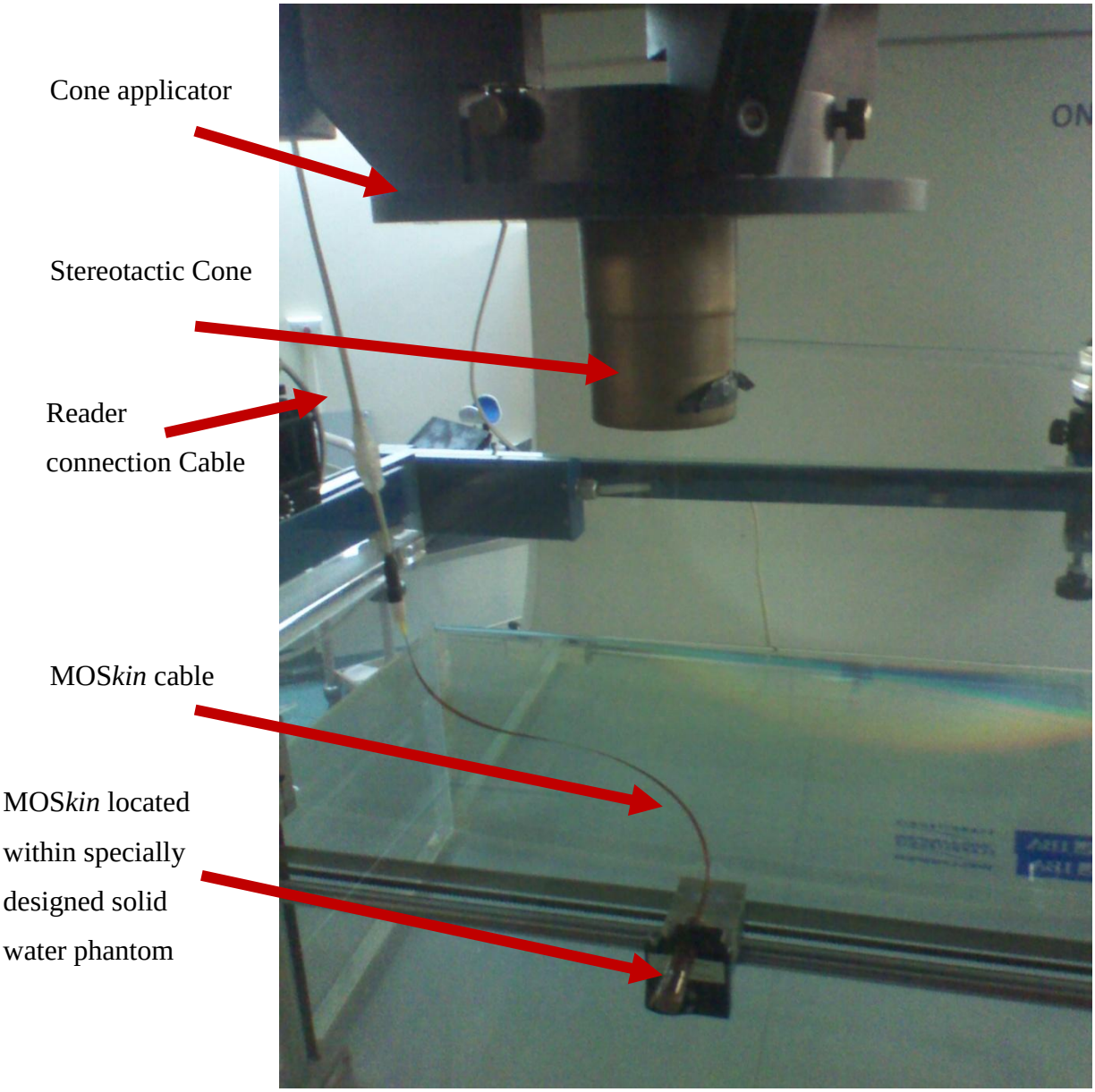

Figure 17: MOSkin set up Face On within the IBA Blue phantom

Edge On

The same protocol was used as for the face on detector except the dosimeter was now rotated 90° clockwise (edge on position). The MOS*kin* was in the same orientation for each edge on profile set up. The edge on beam profile measurements were conducted on cones ranging from a 5 mm to 8 mm in diameter. Turning the MOSkin onto its edge allowed for a smaller sensitive volume to be visible to the beam central axis (CAX). As a result, the resolution of the detector when measuring the dose profile of the respective cone would potentially be smaller than when the MOSkin is placed in its face on position. The beam profiles determined from the edge on set up were compared to their respective face on beam profile.

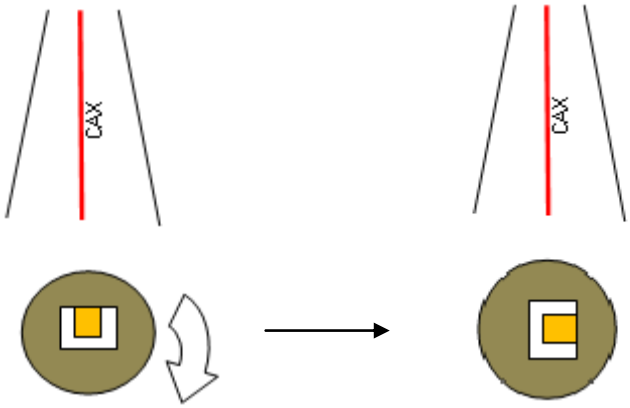

Figure 18: Face on and edge on positioning of the MOSkin. The MOSkin is rotated 90 degrees from its front on position in the clockwise direction for edge on positioning. In both positions, the sensor is centred on the CAX.

3.3.2 IBA Stereotactic Field Diode

The SFD (IBA dosimetry) diode is a p-type diode and is specifically designed for stereotactic and small field measurement. The SFD has an active diameter of 0.6 mm and an active volume thickness of 0.06 mm. The diode was connected to the Wellhofer CU 500E electrometer attached to the IBA Scaditronix Wellhofer water tank with no voltage applied for all measurements.

The SFD was set up in the same way as the MOSkin for beam profile measurements. A reference chamber (RFD^{3G}, PTW-Freiburg) was used. The SFD was positioned with its main axis parallel to the central axis. The light field crosshairs were used initially to centre the SFD. The maximum dose point was then located for the diode in the inline plane. The beam profile was then measured in the cross line plane. Scanning steps of 0.5 mm were used with twenty measurement points taken at each step, which were then averaged. The profile was repeated three times. In order to increase the scanning resolution, the origin point on the cross line was then moved to 0.2 mm and the profile obtained again using the same step size. This was again repeated three times and the average taken. This was conducted to achieve data points at more locations along the beam profile for each cone size.

3.3.3 PTW – Freiburg PinPoint Ionisation Chamber

A small ionisation chamber from PTW-Freiburg, the Pinpoint chamber type 31014 is a fully guarded waterproof air chamber with a central electrode made of aluminium with a diameter of 0.3 mm. The radius of the sensitive volume is 1 mm and it is 5mm long with a sensitive volume of 0.015 cm^3. The wall material is tissue equivalent, consisting of PMMA (0.57 mm) covered with a graphite layer (0.09 mm).

The IBA Wellhofer water tank was used for the measurements. The PinPoint chamber was orientated with its stem perpendicular to the CAX, reducing the amount of scatter reaching the sensitive volume. The ionisation chamber was connected to the Wellhofer CU500E electrometer and microprocessor for beam profile measurements and a nominal voltage of 400 V applied. The same procedure as used by the SFD to measure the beam profile in the cross line plane was implemented. The dosimeter was scanned steps by steps in increments of 0.5 mm with twenty measurements taken and averaged at each position. Each profile was measured three

times and averaged. The chamber was then offset by 0.2 mm and the profiles repeated.

3.3.4 Gafchromic EBT3 Film

EBT3 film has an active layer of 30 µm thickness, which is located between two polyester layers of 125 µm thickness. The process for preparing, reading out and analysing the films was consistent with the procedure used at Prince of Wales Hospital. All measurements were performed using EBT3 films from the same batch. The EBT3 film sheet was cut into 5 cm x 5 cm pieces for both the output and profile measurements. Each film was marked to maintain orientation and scanned using an Epson 10000XL flatbed scanner in a jig to ensure reproducible positioning of the film. The film was positioned in the centre of the flatbed scanner to avoid off axis scanner non-uniformity, and scanned to measure optical density (OD) both prior to exposure to quantify the background image and 24 hours after exposure. ImageJ (*National Institute of Health, Maryland U.S.A)* software was used to analyse films. For profile measurements, the film was placed between slabs of Gammex Solid water with a thickness of 1.5 cm above the film and 10 cm below. The film was placed in an orientation perpendicular to the CAX. For each profile, one exposure was taken and three profiles were extracted. Profiles from the EBT3 film were obtained using a 0.3 mm wide region of interest across the centre of the cone profile. To obtain a similar grey level on the films, the MU was scaled for each field size to deliver 200 cGy at the depth of the film on the CAX. Each film was scanned in transmission mode using 48 bit RGB with a scanner resolution of 300 dpi.

3.4 Output Factor Measurements

As described by Aspradakis et al (2010), output factors describe the relative variation of dose with beam size and are used for dosimetric calculations. The output factor is defined as the ratio of the dose for the field of interest to the dose for the reference field for the same number of MU. This is commonly conducted in a water phantom with the detector placed at a reference depth at the isocentre. The standard protocols AAPM TG 51 and IAEA TRS 398 for absolute dose measurements cannot be reliably performed in the stereotactic beam of the linac used in this study, as reference conditions cannot be met (10 cm x 10 cm is not available).

The method described to measure the output factors using the various dosimeters was taken from current dosimetry protocols: IPEM 103 and DIN 6809-8. An IBA ionisation chamber (IC) with a sensitive volume of 1 cm^3 was used as the reference dosimeter with a Keithley 35040 Advanced therapy dosimeter electrometer (Fluke Biomedical). A warm up beam of 500 MU was delivered to the ionisation chamber before any measurements were conducted. The output factors determined for each dosimeter were compared to in house Monte Carlo calculations, conducted by staff at the Prince of Wales hospital for each cone field size.

3.4.1 MOSkin

The output measurements for all cone sizes were conducted with the one MOSkin in one session. The reference field was taken to be the 4.5 cm diameter cone. The cross calibration was required due to the silicon substrate within the MOSkin, which causes the detector to over respond to Compton scatter present in large fields. In large fields, there is a large dose contribution due to the low energy scattered radiation. In small fields, the dose contribution by this radiation is small and the low energy response is negligible (*PTW 2013*).

Set up for the MOSkin

Source to surface distance (SSD) : 90 cm

Reference depth in water : 10 cm

Cone size range : 0.5 – 4.5 cm

Energy of beam : 6 MV

Beam on delivery : 100 MU

The linac was initially warmed up using three beams of 100 MU each.

The dosimeter was positioned at the location of maximum dose (centre of the radiation field). Up to the 3 cm cone collimator, the positioning of the MOSkin at ΔV_{max} was conducted by measuring the ΔV over the range $\pm$ 0.1 cm from the central axis, down to 0.02 cm increments in both the inline and cross line planes and determining where the maximum signal ($\Delta V_{max)}$ was located. For cone sizes between the 3 cm and 4.5 cm cone, the ΔV_{max} positioning check was not conducted as these field sizes have a relatively large plateau region.

Once the position of ΔV_{max} was determined, the initial threshold voltage (V_0) for the output factor measurements was manually read out. For all cone size measurements, the dose was delivered and read out three times to check reproducibility and reduce the uncertainty of the measurement.

Using the 4.5 cm cone, the ionisation chamber was set up in the same way as the MOSkin. Again, the beam was delivered and the ionisation chamber read out three times with an average taken over the three readings ($IC_{4.5}$) in nano Coulomb's (nC).

The field size was then changed to 10 cm x 10 cm and the same procedure performed

(IC_{10}). The output factor (OF) for the MOSkin over 0.5 – 4.5 cm diameter field sizes ($MOSkin_{dx}$) was then determined using the calculation

$$OF = \frac{IC_{4.5}}{IC_{10}} \times \frac{MOSkin_{dx}}{MOSkin_{4.5}}$$

3.4.2 IBA Stereotactic Field Diode and PTW – Freiburg PinPoint Ionisation Chamber

The same setup and calculation of output factor was used for the SFD and PinPoint ionisation chamber. The SFD and pinpoint chamber were positioned in the centre of the radiation field using the same method used for the MOS*kin.*

3.4.3 Gafchromic EBT3 Film

The film was placed between slabs of solid water with 10 cm build-up and 10 cm backscatter. Each exposure was repeated three times. The same handling and processing methodology as used for profile measurements was again used for output measurements except the scanner resolution used was 75 dpi. The pixel values measured for the red channel of the scanner were used to calculate the net OD for each film piece. A small ROI was taken in the middle of the field for each film and average pixel value determined. The background was subtracted, and the average pixel value was converted to absorbed dose (in cGy) using a previously obtained OD-to dose calibration curve.

4 RESULTS

4.1 MOSkin Linearity of Dose Response

Figure 19 shows the linearity of dose response of the MOSkin for dose ranging from 10-200cGy with an R^2 of 99.79%.

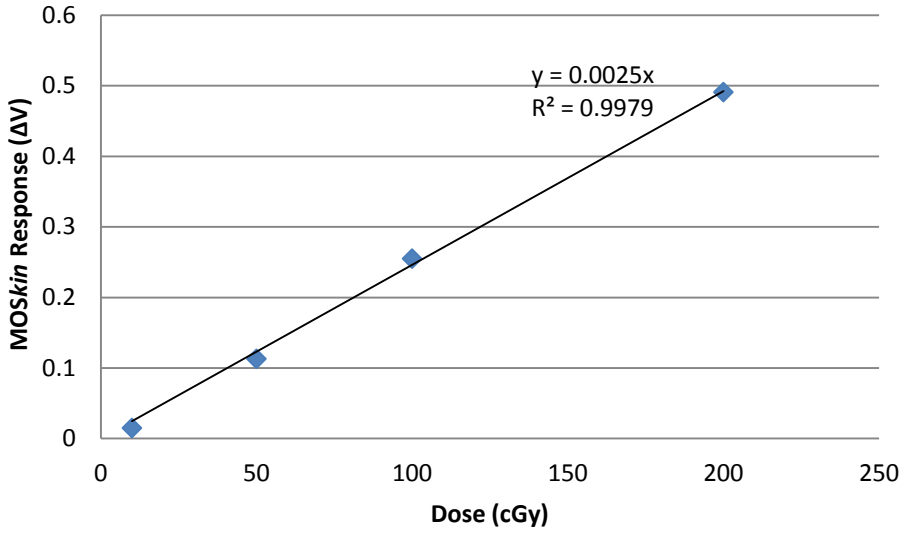

Figure 19. Linearity of dose response for the MOSkin over the range 10 – 200 cGy

4.2 Comparison of beam profiles for the MOSkin in face on and edge on orientation

Other than for the 5 mm cone diameter (figure 20 (a)), the difference in penumbra and FWHM in both face and edge on is unobservable for each respective profile (figure 20 (b) and (c)); however the penumbra width (80% - 20% distance) was consistently larger for the face on MOSkin (figure 22) for all field sizes.

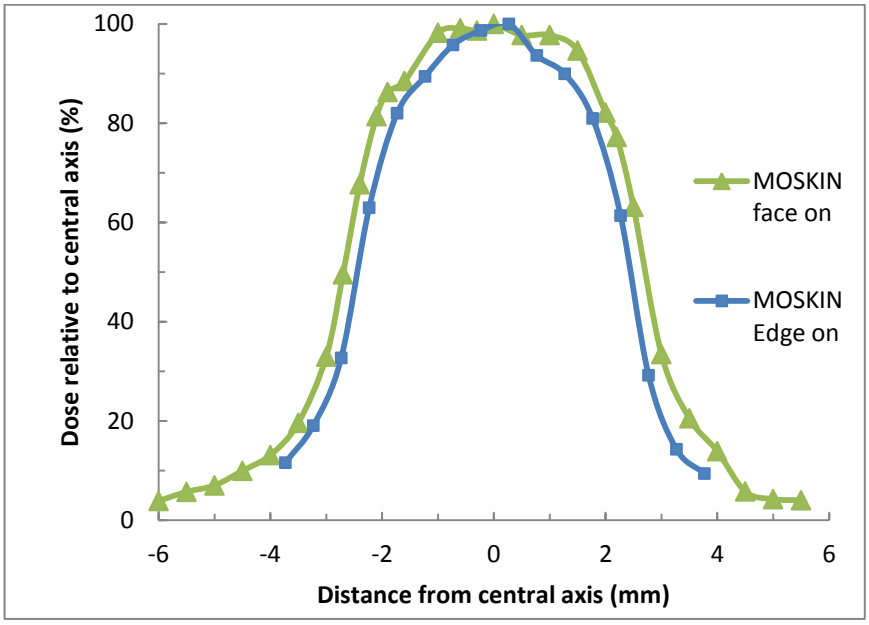
Dose relative to central axis (%)
100
80
60
40
20
0
-6
-4
-2
0
2
4
6
Distance from central axis (mm)
MOSKIN face on
MOSKIN Edge on

(a)

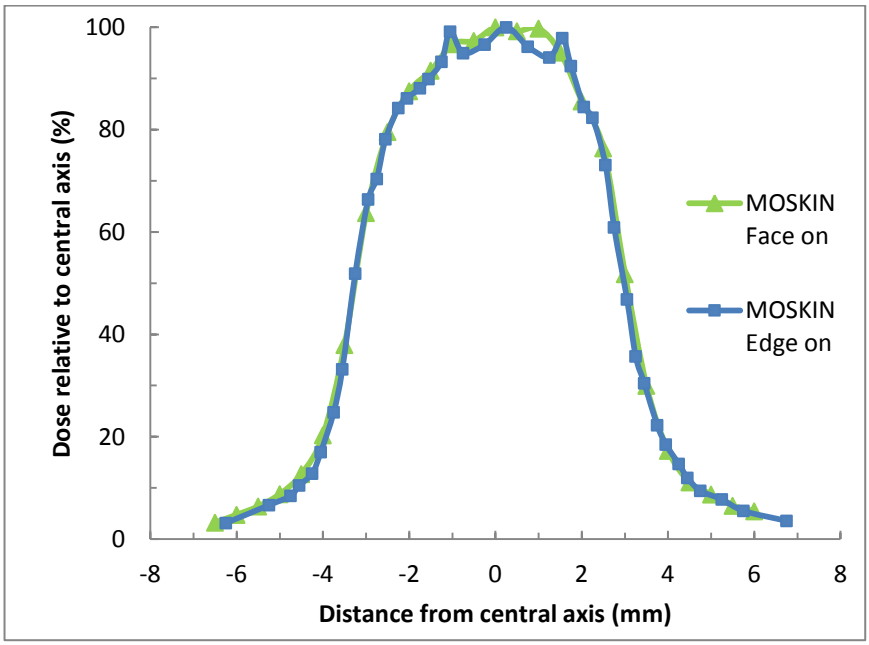
Dose relative to central axis (%)
100
80
60
40
20
0
-8
-6
-4
-2
0
2
4
6
8
Distance from central axis (mm)
MOSKIN Face on
MOSKIN Edge on

(b)

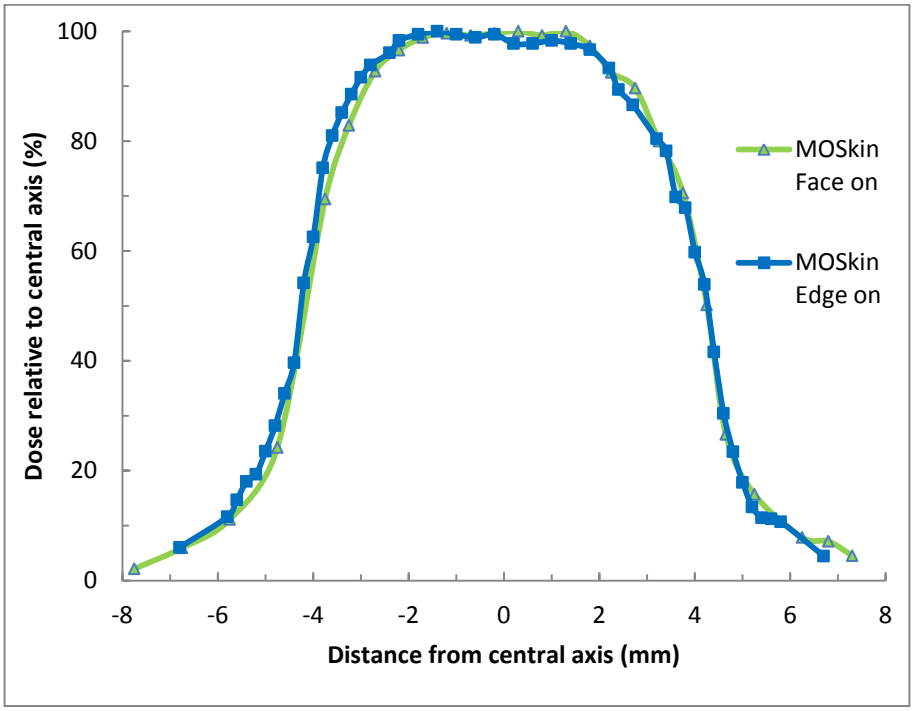

(c)

Figure 20. Measured beam profiles for (a) 5 (b) 6.5 and (c) 8 mm SRS cone diameters for the MOSkin face and edge on . Profiles were centred on the central axis and normalised to 100%

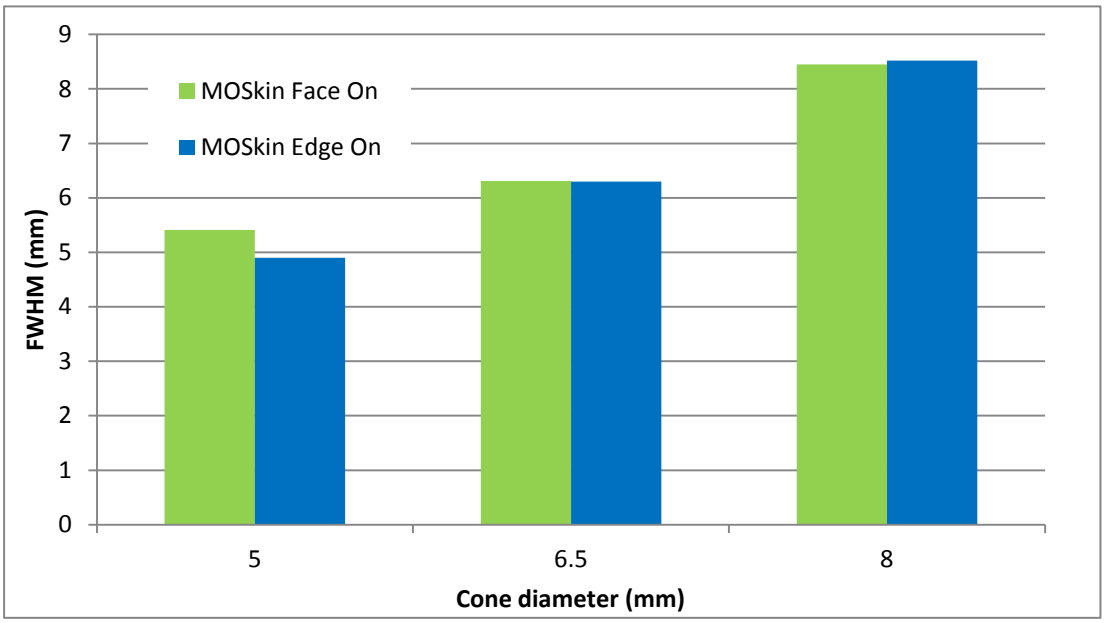

Figure 21. FWHM of the beam profiles using the MOSkin face on and edge on at nominal cone diameters of 5, 6.5 and 8 mm.

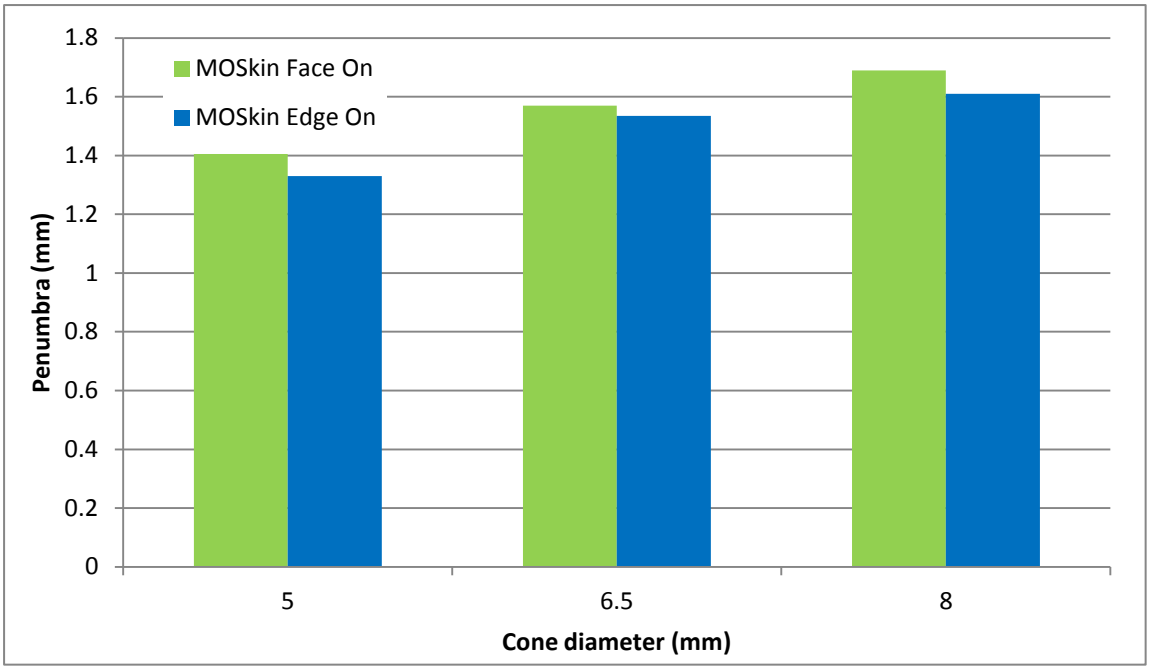

Figure 22. Measured cone penumbral width (80% - 20% dose distance) of the beam profiles for the MOSkin face on and edge on at nominal cone diameters of 5, 6.5 and 8mm. The penumbral width is defined as the distance between the 80% and 20% dose points.

4.3 Comparison of beam profiles between the MOSkin, IBA SFD, PTW PinPoint and EBT3 Film

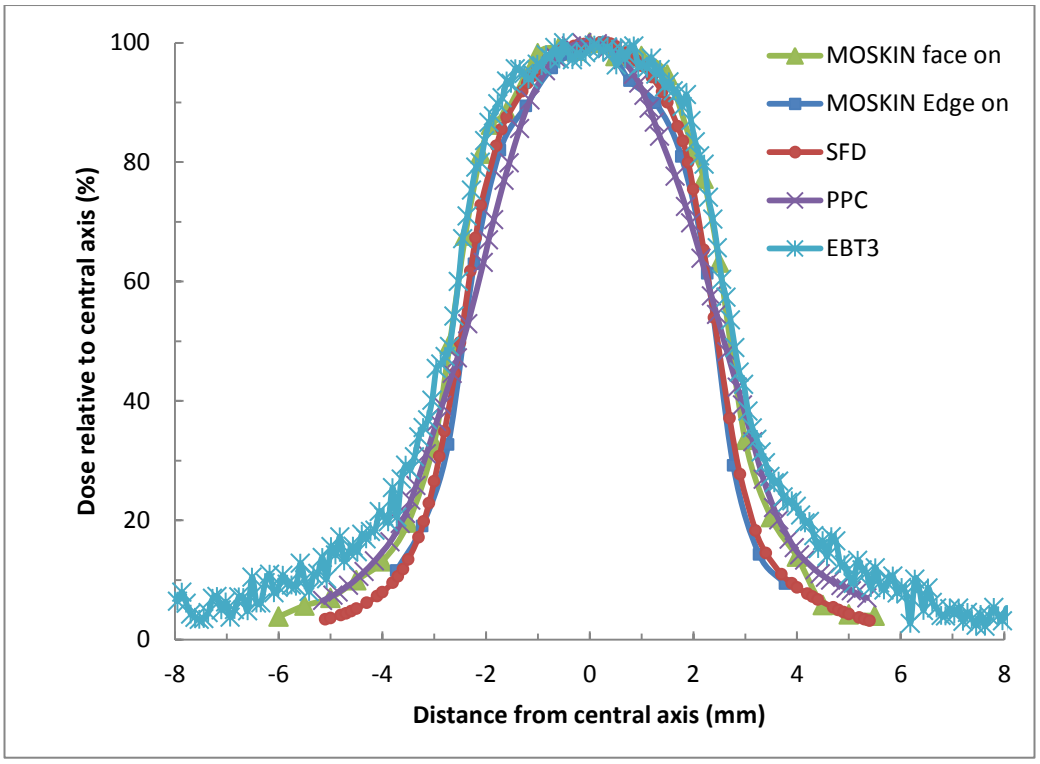

(a)

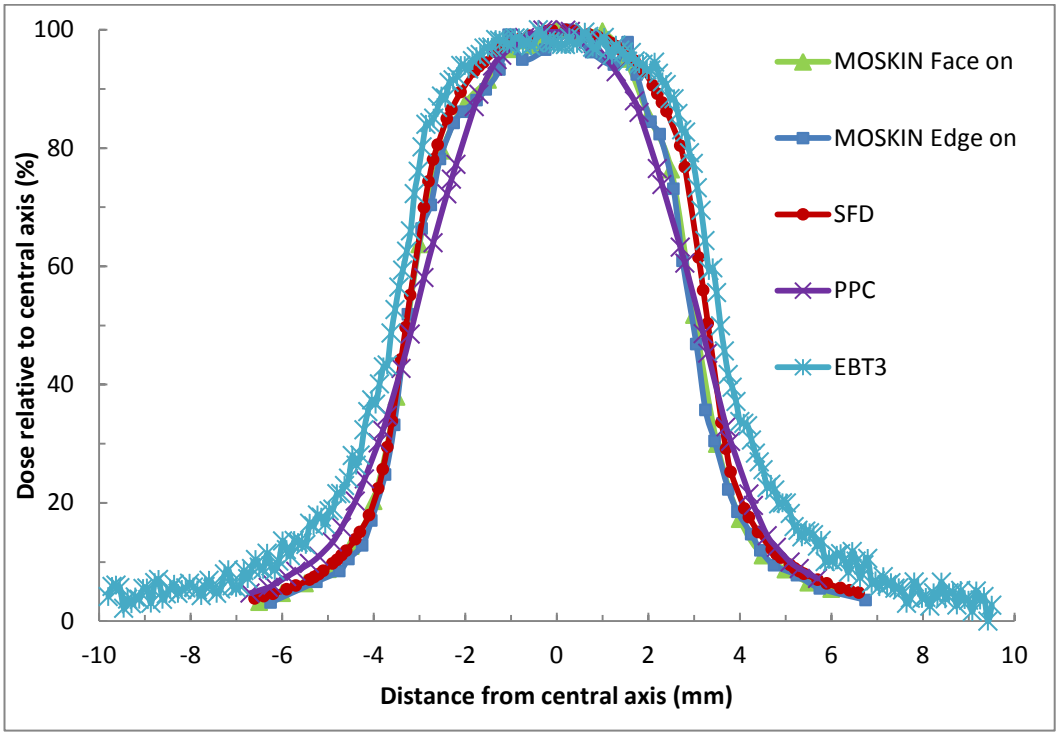
100
80
60
40
20
0
Dose relative to central axis (%)
-10
-8
-6
-4
-2
0
2
4
6
8
10
Distance from central axis (mm)
MOSKIN Face on
MOSKIN Edge on
SFD
PPC
EBT3

(b)

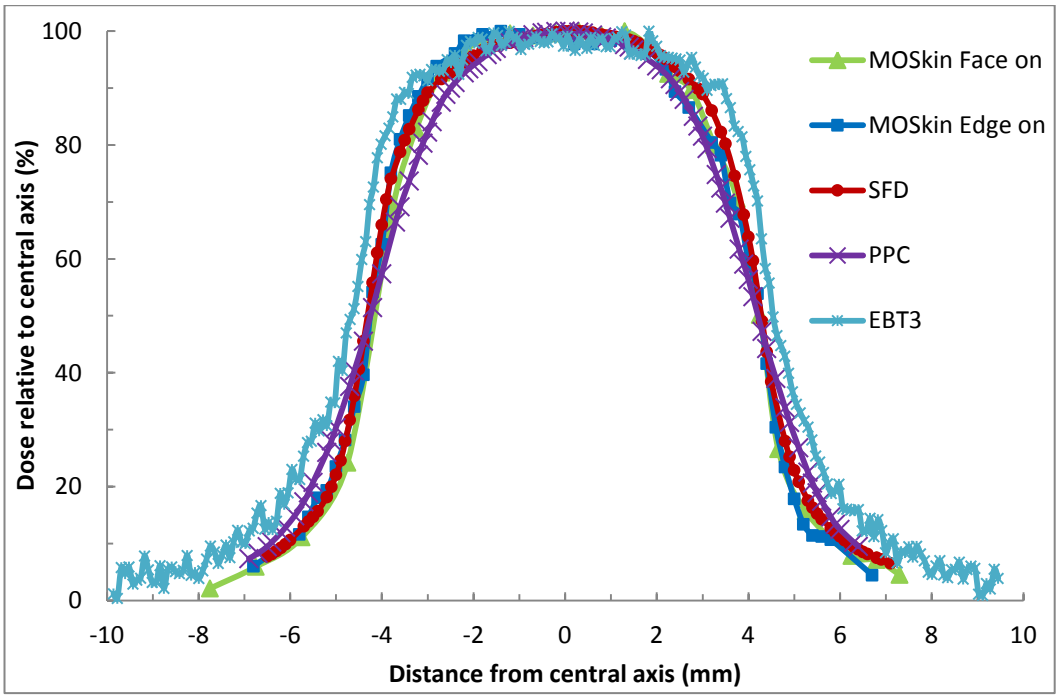
100
80
60
40
20
0
Dose relative to central axis (%)
-10
-8
-6
-4
-2
0
2
4
6
8
10
Distance from central axis (mm)
MOSkin Face on
MOSkin Edge on
SFD
PPC
EBT3

(c)

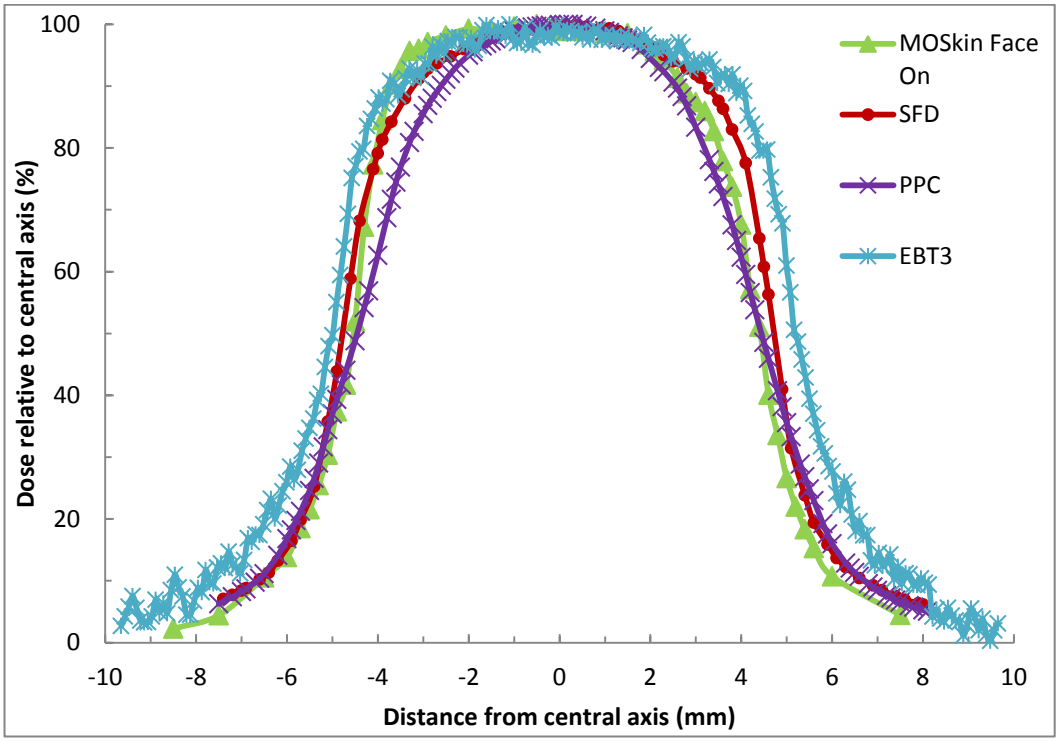
100
80
60
40
20
0
Dose relative to central axis (%)
-10
-8
-6
-4
-2
0
2
4
6
8
10
Distance from central axis (mm)
MOSkin Face On
SFD
PPC
EBT3

(d)

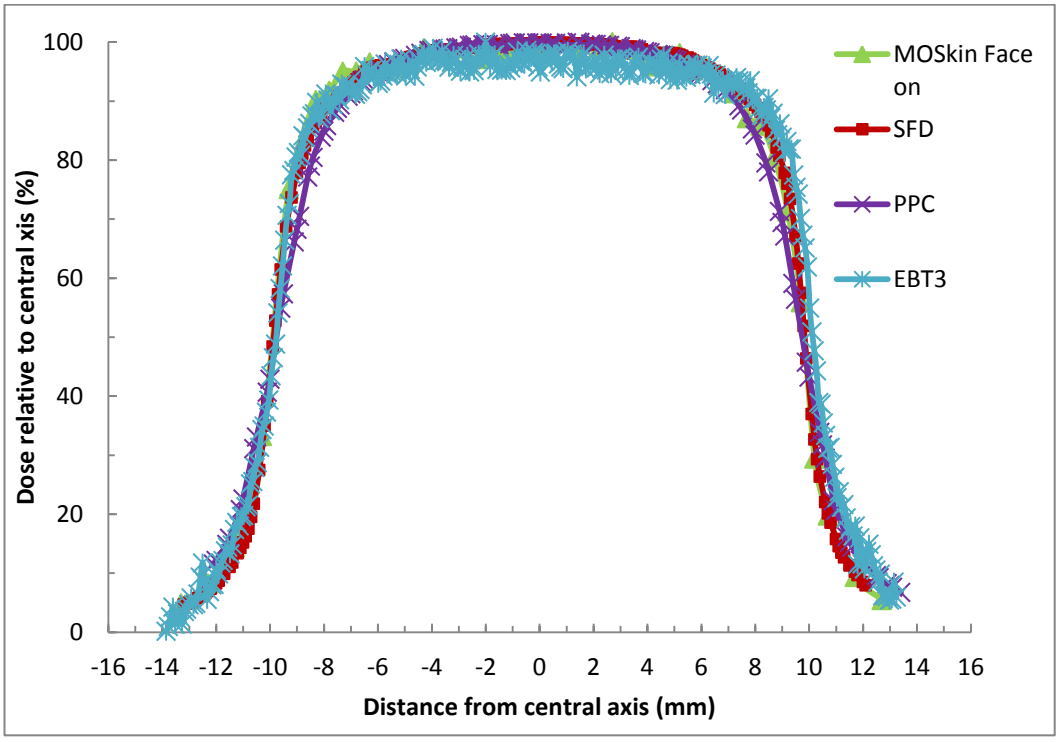
100
80
60
40
20
0
Dose relative to central xis (%)
-16
-14
-12
-10
-8
-6
-4
-2
0
2
4
6
8
10
12
14
16
Distance from central axis (mm)
MOSkin Face on
SFD
PPC
EBT3

(e)

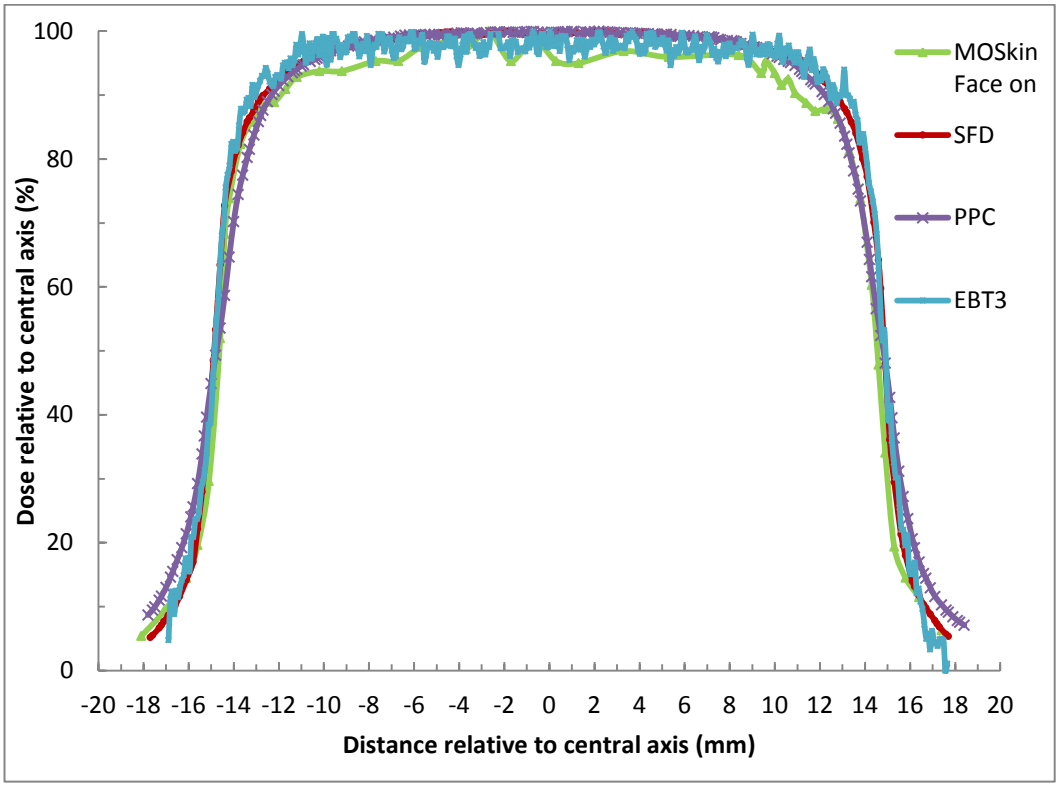

(f)

Figure 23. Measured beam profiles for (a) 5 (b) 6.5 and (c) 8 (d) 10 (e) 20 and (f) 30 mm nominal cone diameters for the MOSkin, SFD, PPC and EBT3. Profiles were centred on the central axis and normalised to 100%

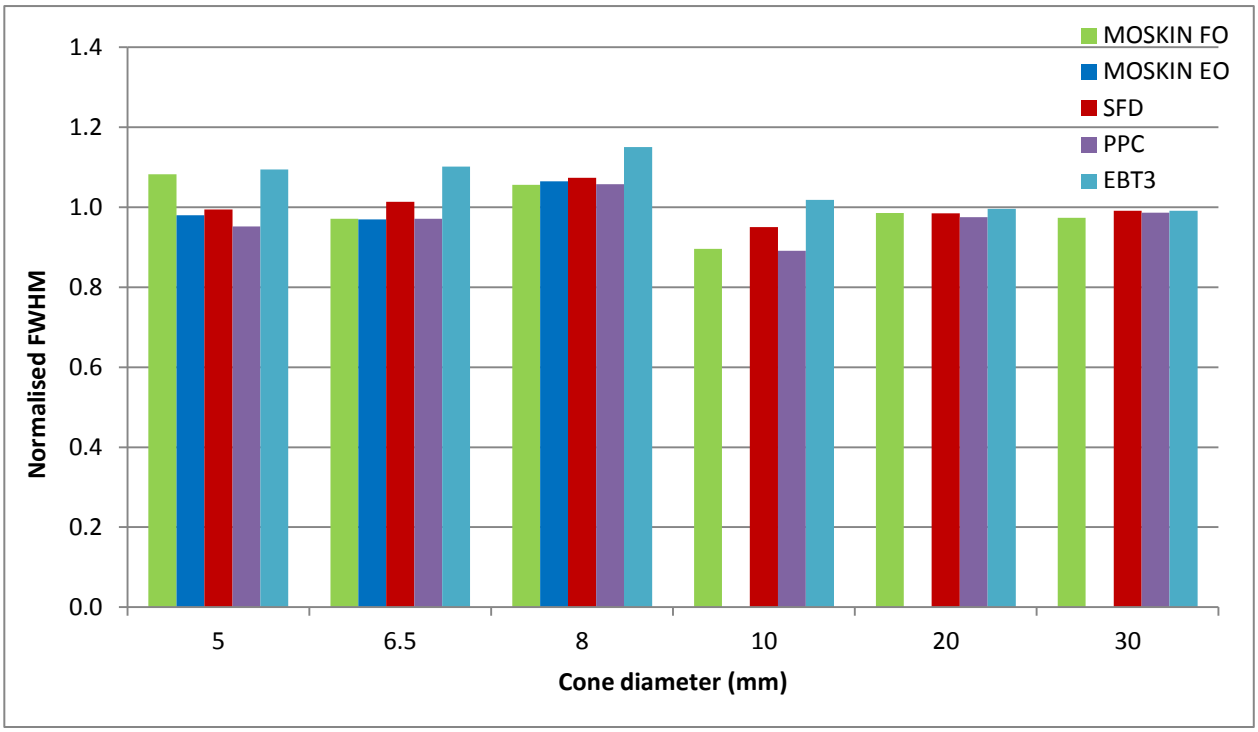

Figure 24. The FWHM for beam profiles of the MOSkin, SFD, PPC and EBT3 is normalised to the expected value at nominal cone diameters of 5, 6.5, 8, 10, 20 and 30 mm.

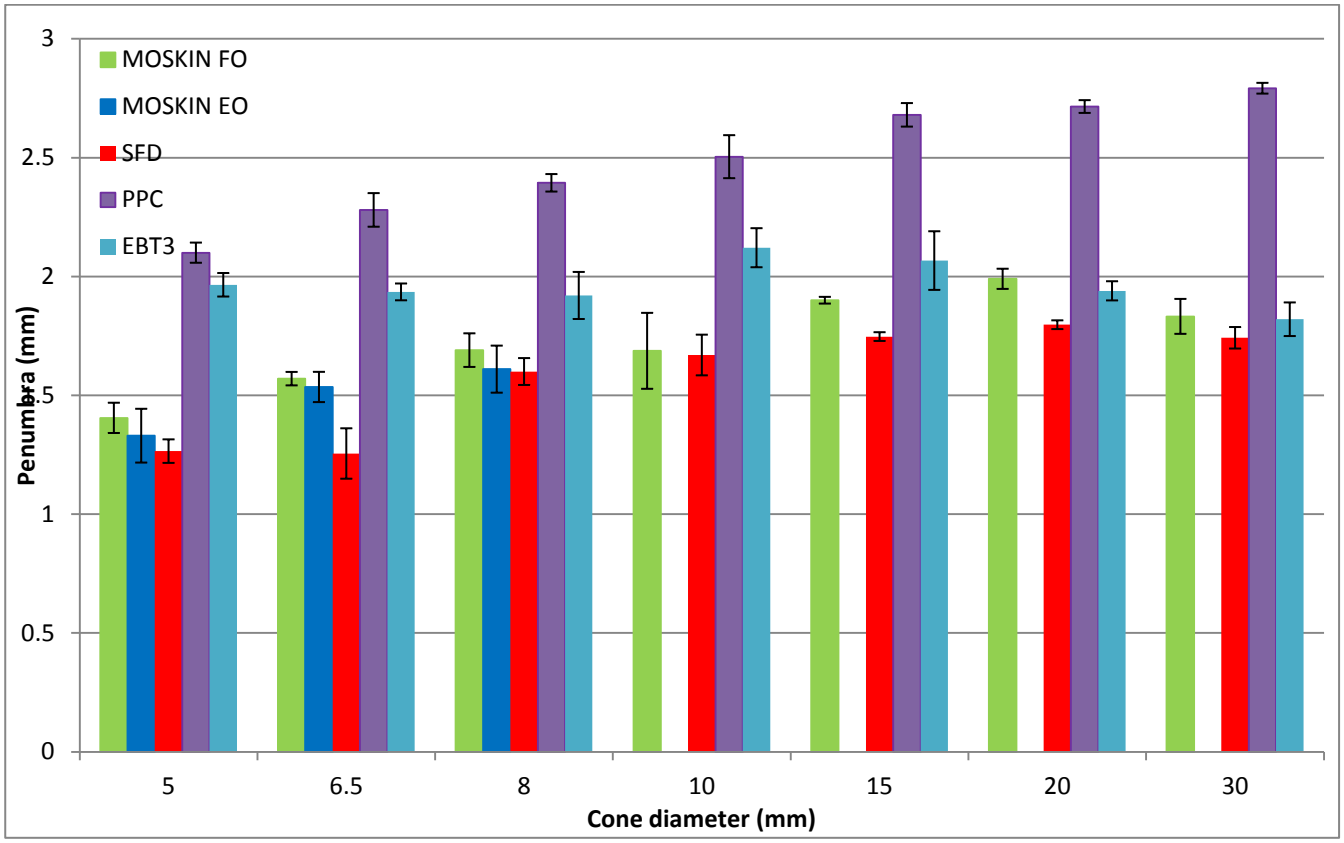

Figure 25. Penumbral width (80% - 20% dose distance) of the beam profiles for the MOSkin, SFD, PPC and EBT3 at nominal cone diameters of 5, 6, 8, 10, 20 and 30 mm. Uncertainty bars represent 1 standard deviation in measurement

Each beam profile was measured three times. The uncertainty bars define 1 standard deviation from three measurements of the 80%-20% penumbra, which includes uncertainty of the penumbra measurement on the left and right side of the beam profile for each dosimeter assuming a symmetrical beam profile.

Table 1. The Coefficient of Variance (CoV) for penumbra width (80% - 20%) dose distance

Dosimeter	CoV (%)
MOSkin face on	13.0
IBA SFD	15.1
PTW PinPoint	10.7
EBT3	5.1

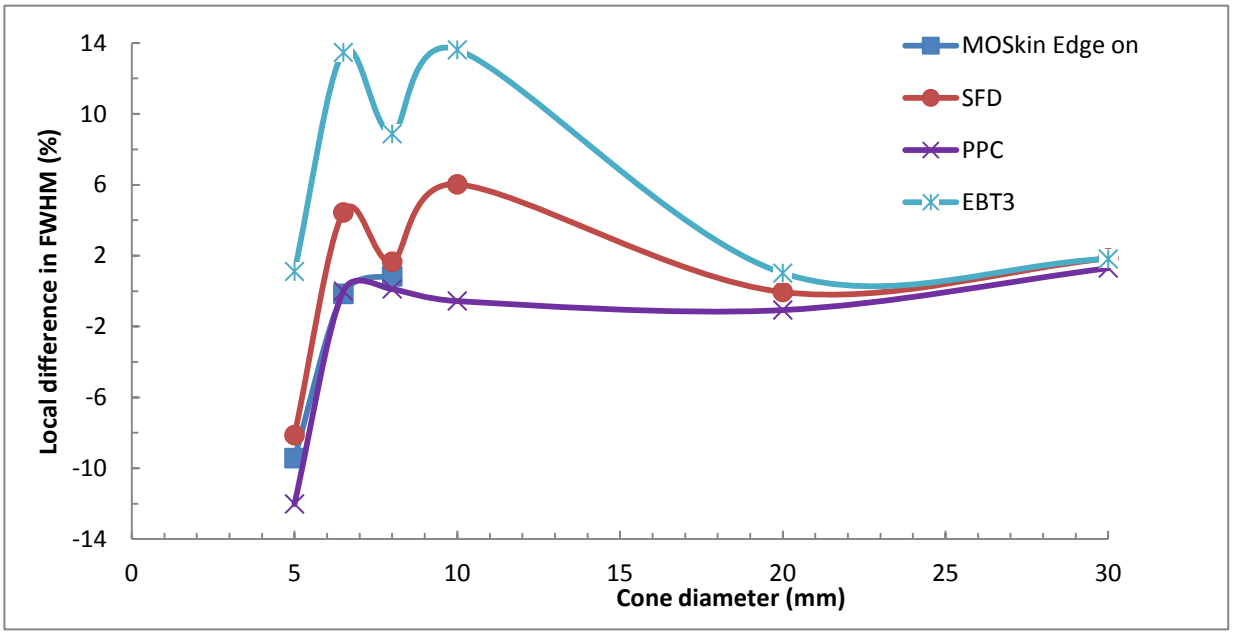

Figure 26.Percentage difference in FWHM relative to the MOSkin face on for the SFD, PPC, MOSkin edge on and EBT3 at nominal cone diameters of 5, 6, 8, 10, 20 and 30 mm. The MOSkin edge on profile was measured only up to the 8 mm cone diameter.

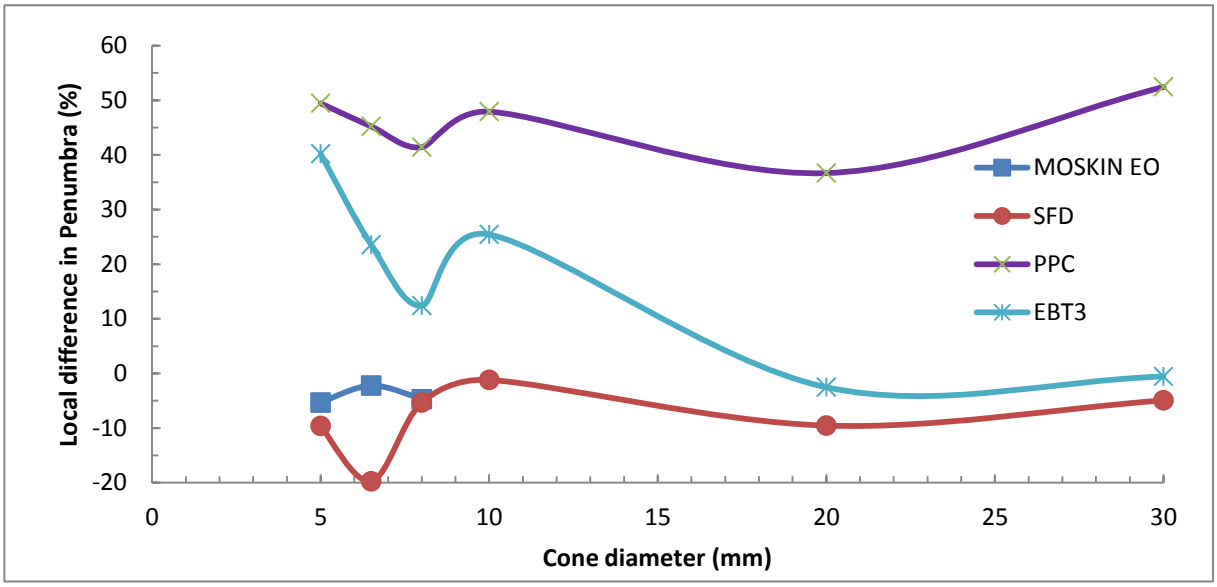

Figure 27. Percentage difference in penumbral width (80% - 20% dose distance) relative to the MOSkin face on for the SFD, PPC, MOSkin edge on and EBT3 at nominal cone diameters of 5, 6, 8, 10, 20 and 30 mm. The MOSkin edge on profile was measured only up to the 8 mm cone diameter.

4.4 Output factors: comparison between the MOSkin, IBA SFD, PTW PinPoint and EBT3 Film

In house Monte Carlo output factor data for a 6 MV beam for the stereotactic cones used were available for comparison to the respective values determined for all four dosimeters used in the measurements (Figure 28). The uncertainty bars represent 1 SD of three repeated measurements of the output at each field size. The percentage difference between the expected output factor value and the measured are shown in figure 29. The percentage differences between the

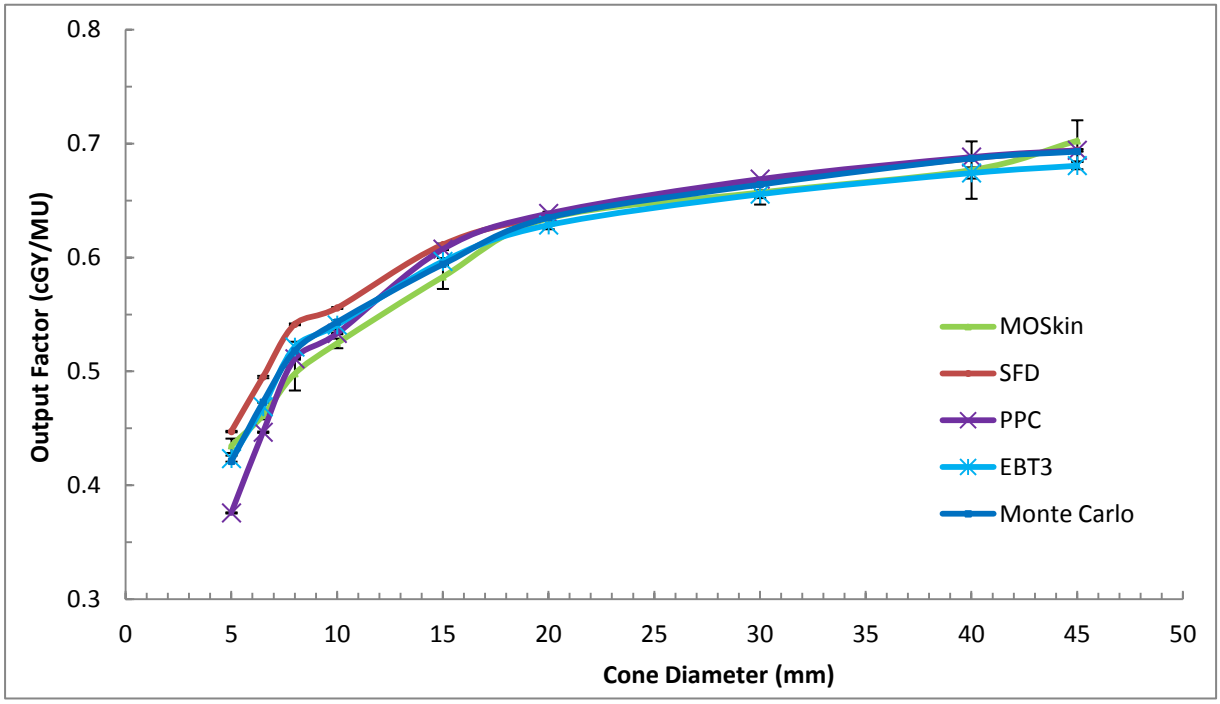

MOSkin and the SFD, PinPoint and EBT3 are also shown in figure 30.

Figure 28. Output factors obtained using the MOSkin, SFD, PPC, EBT3, and in-house Monte Carlo calculations for nominal cone diameters of 5 mm to 45 mm. Error bars represent 1 standard deviation in measurements.

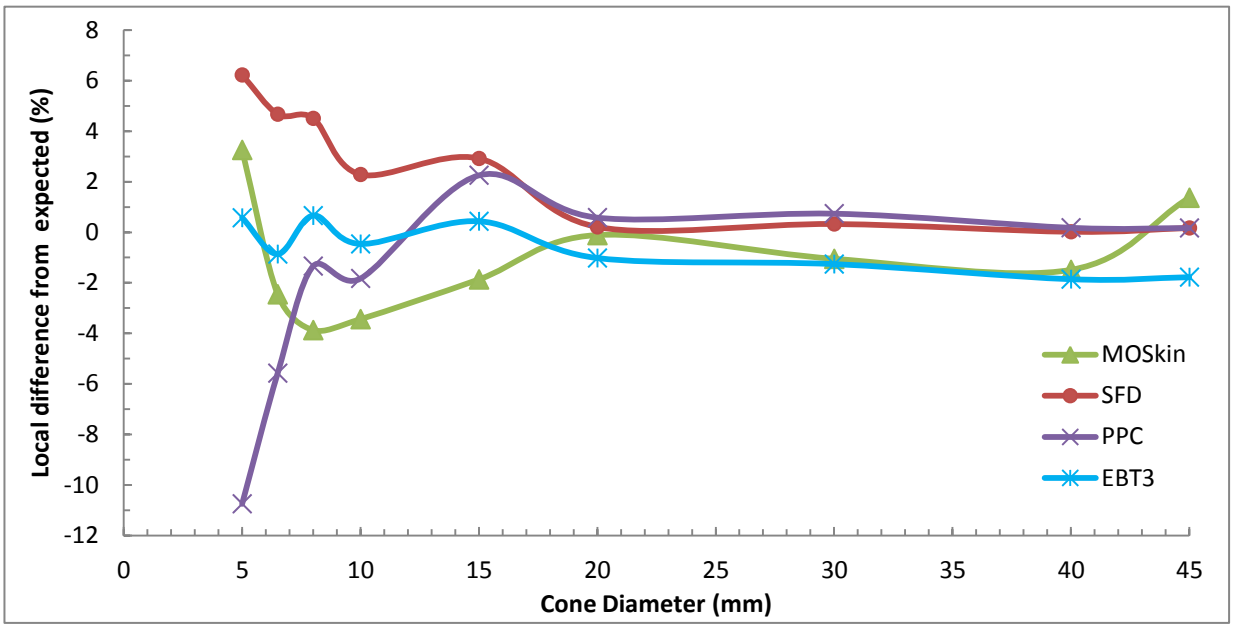

Figure 29. Percentage difference between in-house Monte Carlo calculated values and the MOSkin, SFD, PPC and EBT3 film for output factor values.

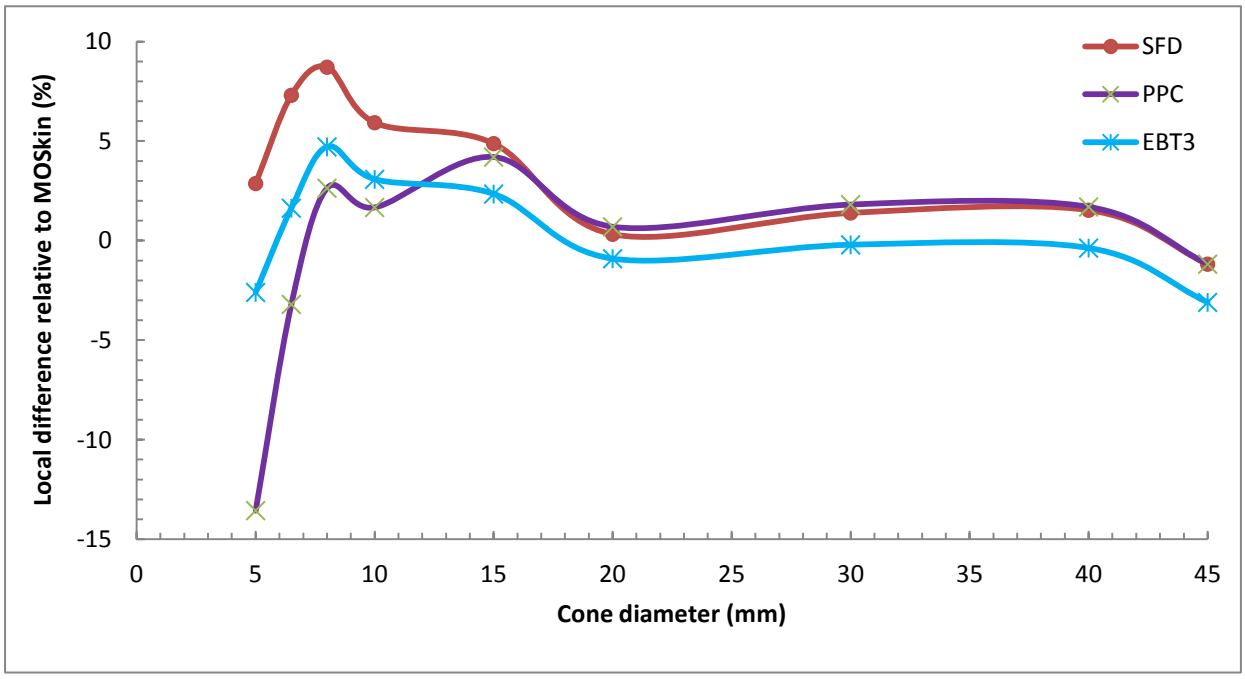

Figure 30. Percentage difference between the MOSkin and the SFD, PPC and EBT3 film output factor values

DISCUSSION AND CONCLUSION

In this work, MOSkin, SFD, PinPoint ion chamber and radiochromic film (EBT3) were used for profile measurements of 6 MV stereotactic beams of 5 mm to 30 mm in diameter. Output factors were also determined for the detectors up to a field size of 45 mm.

The MOSkin exhibited a linear dose response over the range 10 cGy to 200 cGy with a fit with R^2 of 99.79% (Figure 19). The dose delivered to the MOSkin when measuring beam profiles was guided by the uncertainty of the measurement. Consequently, as the profile moved into the penumbra and the tail, the dose delivered was increased to reduce the uncertainty. The linear dose response allowed for a simple ratio correction to produce the overall beam profile.

With the MOSkin in an edge on position, the expectation was for a more 'true' beam profile to be measured relative to the MOSkin in a face on position for the stereotactic fields, specifically field diameters of less than 10 mm. This was due to the smaller detector size visible to the direct beam when in the edge on position, which could potentially increase resolution and reduce the volume averaging effect. As explained thoroughly within the literature review, the effect that the detector size has on the ability to provide accurate beam profile measurements is volume averaging. The volume averaging effect causes an artificial broadening of the penumbra, which adds to the broadening of the penumbra caused by lateral charged disequilibrium within small fields.

When comparing the MOSkin in edge on and face on positioning for beam profile measurements, it is only at the 5 mm field size that a difference in profile is evident (Figure 20). The dose profiles have been analysed via the full width half maximum

(FWHM) and the penumbral width (80% - 20% dose distance). There was a difference in FWHM of 0.5 mm between the two beam profiles for the 5 mm field size (Figure 21). The FWHM of the two beam profiles was -0.1 mm and 0.4 mm from the nominal field size for the edge on and face on MOSkin respectively. At field diameters of 6.5 mm and 8 mm no obvious difference in FWHM was seen comparing the MOSkin in the two orientations. The FWHM in both MOSkin positions varied from the nominal field sizes of 6.5 mm and 8.5 mm by -0.2 mm and 0.5 mm respectively.

The average penumbral width taken over the 80% - 20% distance was consistently larger for the MOSkin in the face on position (Figure 22). The average penumbra width for the MOSkin in the face on position was 1.6 mm, in comparison to the edge on position, which was 1.5 mm. The percentage difference between the measured penumbra widths was 4%, with the largest difference of 5.3% at the 5 mm field size. These results indicate that the initial hypothesis was correct, i.e. the MOSkin edge on relative to the MOSkin in the face on position reduces the artificial broadening of the penumbra in stereotactic field sizes due to the improved spatial resolution.

As has been described in the literature review, the ion chamber is typically not recommended for small field measurements (*Aspradakis et al 2010*). Our results agreed with the literature, with the PinPoint chamber broadening the penumbra with respect to the other dosimeters for all field sizes (Figures 23 and 25). The PinPoint chamber had been recommended (*PTW Freiburg 2011*) for use in small field dosimetry down to a field diameter of 20 mm, however, broadening of the penumbra was still evident in both the 20 mm and 30 mm field size beam profiles (Figure 25). An initial sharp gradient or dose fall off is seen with respect to the other dosimeters, which flattens as the dose drops below 50% relative to the dose at the central axis.

The penumbral width of the PinPoint dosimeter is on average, 0.8 mm larger than the MOSkin in the face on and edge on position over their respective measured field sizes.

The use of diodes has been recommended by Aspradakis *et al* (2010) for small field dosimetry due to their relatively small sensitive volumes compared to ionisation chambers. The SFD has the smallest penumbra width for all beam profiles measured (Figure 25). In comparing the MOSkin to the SFD, the penumbral width was always within ± 0.3 mm for all field sizes (Figure 25). Excluding the 8 mm beam profile, the penumbral width was within ± 0.2 mm. No trend was obvious for the variation in penumbral width between the SFD and MOSkin, as this fluctuated for all beam profiles; however, the overall average penumbra width for both the SFD and MOSkin were equal, with an average of 1.56 mm (Figure 27). The coefficient of variance (CoV) was also similar, with a CoV of 15% and 13% respectively (Table 1). Radiochromic film has the ability for very good spatial resolution as it is determined by the resolution of the film scanner. With this in mind, the broad penumbras for beam profiles obtained using film are unexpected (Figure 23 and 25). The penumbra width for beam profiles for field sizes 5 mm, 6.5 mm, 8 mm and 10 mm measured with EBT3 film are consistently larger with respect to the MOSkin. The difference between the MOSkin and EBT3 is largest for the 5 mm field size, with the penumbra approximately 40% wider for EBT3 film (Figure 27). The difference in penumbra width decreases once the 10 mm field size is reached, with the penumbra width approximately equivalent at the 30 mm field diameter. The average penumbra width for EBT3 film is 1.95 mm, which is 0.39 mm larger than for both the MOSkin and the SFD. The CoV for EBT3 with respect to the penumbra width over the measured field sizes was 5%. A high resolution was used to read the beam profiles by the

scanner, which ensured a very high sample size and data points for each profile; however, broadening of the penumbra is seen for EBT3 film up to 10 mm field sizes. EBT3 film is typically taken as the gold standard for small field dosimetry due to their high resolution (*Hassani et al 2014*), therefore the artificial broadening of the penumbra could be due to incorrect background subtraction or scanner issues.

Comparing the FWHM values for all dosimeters, the SFD showed the least overall difference with respect to the nominal field sizes (Figure 24). The difference between detector FWHM and nominal FWHM fluctuated for all dosimeters over all field sizes. Excluding the 10 mm field size, the variation between the nominal and measured field size was less than 0.5 mm for the MOSkin. At the 5 mm field size, a large variation in FWHM measurement is seen between the dosimeters, specifically the PinPoint chamber and the MOSkin with a FWHM of 4.76 mm and 5.4 mm respectively. If the initial results taken with the MOSkin in the edge on position are compared to the PinPoint regarding FWHM, a difference of 0.14 mm is calculated for the 5mm field size.

This result is also consistent for the SFD as the difference in the FWHM for the SFD and the MOSkin face on is 0.44 mm, whilst for the MOSkin edge on, the difference is 0.07 mm. The edge on MOSkin measurements were only conducted up to the 8 mm field size, therefore the profiles from the 10 mm field size and above cannot be compared with the edge on MOSkin. The percentage difference in FWHM between the MOSkin in the face on position and the other dosimeters tend to decrease for field sizes larger than 10 mm. For both the 20 mm and 30 mm field size, the FWHM values obtained using all types of dosimeters are within ± 1% of corresponding MOSkin data.

Our data suggests that the PinPoint chamber should not be used for beam profile measurements at small field sizes, which agrees with the literature *(Tyler et al 2013, Aspradakis 2010).* The PinPoint chamber was seen to broaden the penumbra for all field sizes measured. The MOSkin in the face on position was seen to agree with the SFD penumbra width values above the 8 mm field size, whilst the MOSkin in the edge on orientation was more consistent with penumbral width values from the 5mm to 8 mm field diameter range. The EBT3 film results show that the penumbra has been broadened with respect to the SFD and the MOSkin in both orientations for field sizes of 10 mm and below.

Of the four dosimeters, only radiochromic EBT3 film is considered to be water equivalent. The remaining dosimeters may require correction of measured output factors to account for dose perturbation caused by the non-water equivalent components. EBT3 radiochromic film correlates well with the Monte Carlo calculated data, specifically for cone sizes below 20 mm (Figure 28). For cone sizes of 20 mm and larger, the EBT3 film underestimates the output factor relative to the Monte Carlo values (Figure 29). When EBT3 film is compared to the MOSkin, the MOSkin exhibits an over response for the output factor at the smallest field size of 5 mm (Figures 28, 29 and 30). This over response (2.6%) is consistent with other published data (Tyler *et al* 2013, Morin *et al* 2013) and is suggested to be due to its silicon components. Scott *et al* (2012) attributed this over response to the high density of silicon ($\rho = 2.33$ gcm^3) with respect to water ($\rho = 1.00$ gcm^3).

The MOSkin underestimates the output ratio over cone diameters 6.5 mm to 40 mm compared to the Monte Carlo measurements, ranging from -3.9% to -0.1% with the MOSkin values tend to be in better agreement with Monte Carlo simulated data with increasing cone diameter. Czarnecki and Zink (2013), however, have shown

that diodes may underestimate the dose at the larger fields, yet overestimate the dose at the smaller field sizes. They explained that this effect may be caused by the increasing ratio of the mass energy absorption coefficient for 6 MV beams; however this should be further investigated for the MOSkin. This underestimation is not seen using the SFD, which is also a silicon based dosimeter. The non-water equivalent SFD over responds at the smallest field sizes due to the dose perturbation and dose overestimation *(Tyler et al 2013).* The percentage difference decreases, however, to a maximum of 0.3% once the 20 mm field size is reached (Figure 29).

The PinPoint chamber underestimates the dose below the 10 mm field size (Figure 28), which agrees with reported data (Czarnecki et al 2013)). The largest percentage difference is seen at the smallest field size, with an under response of 10.7% and 13.6% relative to the Monte Carlo and MOSkin values respectively. The underestimation and dose perturbation is most likely a volume averaging effect. At a cone diameter of 8 mm, the PinPoint over responds to dose with respect to the MOSkin, and the difference increases with increasing cone diameter.

A correction factor needs to be determined for the SFD, PinPoint and MOSkin, if they are to be used for small field output measurements, especially below 20 mm field size. If the average output ratio is calculated over all four dosimeters, the maximum percentage difference between the average and Monte Carlo value would be ±1.1% over all cone diameters. The method of using several dosimeters to conduct the measurement and take an average has been discussed in other published work (*Aspradakis et al 2010)*; however the accuracy of this method using the SFD, PinPoint, EBT3 and MOSkin dosimeters to determine accurate data should be investigated further.

Conclusion

The small fields used in stereotactic radiation therapy/surgery (SRT/SRS) are dosimetrically challenging in ways that are not encountered for larger fields including the volume averaging effect, lateral electron disequilibrium and source occlusion.

In this work, the use of the CMRP designed MOSkin as a possible small field dosimeter for use in SRS/SRT was studied. The MOSkin was compared and analysed against dosimeters that have been defined for use in small field dosimetry, including the latest Gafchromic film (EBT3), the IBA stereotactic field diode and the PTW PinPoint chamber in terms of beam profile and output factor measurements.

The MOSkin exhibited a linear dose response up to 200cGy. Beam profile measurements were conducted using 6 MV x-ray beams of 5 mm up to 30 mm in diameter using in house built stereotactic cones. The MOSkin was identified to resolve the penumbra region quite accurately in both face on and edge on orientations in comparison to the SFD and EBT3 film. The application of the MOSkin in the edge on orientation identified better resolution of the penumbra in the smallest field sizes, which could result from the smaller detector size visible to the x-ray beam in comparison to the MOSkin in the face on position. The PinPoint chamber was shown to broaden the penumbra in the smaller field sizes and the volume averaging effect could still be seen at cone field sizes above 20 mm. Unless the dose perturbation due to the volume averaging effect are corrected for, the PinPoint chamber should not be used for beam profile measurements in stereotactic small fields.

In the case of output factors, it was shown that both silicon based dosimeters, the SFD and the MOSkin over responded at the smallest field size of 5 mm. The EBT3

film corresponded well with output factor values determined by in-house Monte Carlo calculations, possibly due to its water equivalence; however the film had a slight under response at field sizes above 20 mm. The PinPoint chamber under responded significantly at the 5mm cone field size, which could be explained by its relatively large volume. If the output ratio was averaged for all four dosimeters, there was minimal variation between the Monte Carlo values for all field sizes. This gives basis for the use of a variety of dosimeters to conduct output factor measurements, which could increase the accuracy in output factor values for small fields.

In conclusion, the MOSkin dosimeter can provide relatively accurate profile data for very small beams used in stereotactic radiosurgery or radiotherapy since it can overcome, to some extent, the problems related to the finite size of conventional detectors. With reference to output factor values in small fields, to increase assurance in results and accuracy, a number of dosimeters should be used, which could include the MOSkin; however this requires further study and investigation.

REFERENCES

AAPM (2004), *Profile of Radiation Oncology Departments*, AAPM Survey

Almond, P. R. et al (1999), *AAPM TG-51 protocol for clinical reference dosimetry of high energy photon and electron beams*, Medical Physics, Vol. 26, pp. 1847 - 1870

Apradakis, M. et al (2010), *Small field MV photon dosimetry*, Report Number 103, IPEM, York, UK

Aspradakis, M, Byrne, J. (2011), *Small field dosimetry: challenges and progress*, http://medicalphysicsweb.org/cws/article/opinion/45334, accessed 5/2014.

Attix, F.H (1986), *Introduction to Radiological Physics and Radiation Dosimetry*, Wiley and Sons, New York, USA

Benmakhlouf, H. et al (2014), *Output correction factors for nine small field detector in 6MV radiation therapy photon beams: A PENELOPE Monte Carlo study*, Medical Physics, Vol. 41, pp. 041711-1/12

Benson, C. et al (2004), *Radiation induced statistical uncertainty in the threshold voltage measurement of MOSFET dosimeters*, Physics in Medicine and Biology, Vol. 49, pp. 3145-3159

Bouchard. H. et al (2009), *Ionisation chamber gradient effects in nonstandard beam configurations*, Medical Physics, Vol. 36, pp. 4654-4663

Bower, M.W. and Hintenlang, D.E. (1998), *The characterization of a commercial MOSFET dosimeter for use in diagnostic radiology*, Health Physics Society, Vol. 75, pp 197-204

Brunet-Benkhoucha, M. et al (2011), *Clinical Impact of detector selection in small photon beam modelling*, Medical Physics, Vol. 38, p 3615

Bucciolini, M. et al (2003), *Diamond detector versus silicon diode and ion chamber in photon beams of different energy and field size*, Medical Physics, Vol. 30, pp 2149-2154

Bushberg, J.T. et al (2010), *The Essential Physics of Medical Imaging*, Third Ed., Lippincott Williams and Wilkins, Philadelphia, USA

Butson, M.J, et al (2010), *Energy response of the new EBT2 radiochromic film to x-ray radiation*, Radiation Measurements, Vol. 45, pp. 836-839

Casanova, B.V, et al (2013), *Dosimetric characterisation and use of Gafchromic EBT3 film for IMRT dose verification*, Journal of applied clinical medical physics, Vol. 4, pp 158-17

Cheung, T., Butson, M. J. and Yu, P. K (2004), *Effects of temperature variation on MOSFET dosimetry*, Physics in Medicine and Biology, Vol. 49, N191-N196

Chine, L.S., Regine, W.F. (2008), *Principles and Practice of Stereotactic Radiosurgery*, Springer Science and Business Media, New York, USA

Czarnecki, D and Zink, K. (2013), *Monte Carlo Calculated correction factors for diodes and ion chambers in small photon fields,* Physics in Medicine and Biology, Vol. 58, pp. 2431-2444

Das, I., Ding, G.X. and Ahnesjo, A. (2008), *Small Fields: Nonequilibrium radiation dosimetry*, AAPM, Vol. 35, pp 206-215

Dasu, A. et al (1998), *Liquid ionisation chamber measurements of dose distributions in small 6 MV photon beams*, Physics in Medicine and Biology, Vol. 43, pp. 21-36

DIN 6875-1 (2004), *Special Radiotherapy Equipment - Part 1: Percutaneous stereotactic radiotherapy, basic performance characteristics and essential test methods*, German National Standards, Berlin

Duggan, D.M. and Coffey, C.W, *Small photon field dosimetry for stereotactic radiosurgery,* Medical Dosimetry, Vol. 23, pp. 153-159

Gagnon, J.C et al (2011), *Dosimetric performance and array assessment for plastic scintillation detectors for stereotactic Radiosurgery quality assurance,* Medical Physics, Vol. 39, pp 429-436

Gambarini, G. et al. (2013), *Online in vivo dosimetry in high dose rate prostate brachytherapy with MOSkin detectors: In phantom feasibility study,* Applied Radiation and Isotopes, 83 (Part C), pp. 222-226

Grebe, G. et al. (2001), *Dynamic arc radiosurgery and radiotherapy commissioning and verification of dose distributions*, International Journal of Radiation Oncology, Biology and Physics, Vol. 49, pp. 1451-1460

Hall, E.J and Giaccia, A.J. (2006), *Radiobiology for the Radiologist*, Sixth Ed., Lippincott Williams and Wilkins, Philadelphia, USA, pp. 5-15

Hardcastle, N. et al (2011), *High dose per fraction dosimetry of small fields with Gafchromic EBT2 film,* Medical Physics, Vol. 28, pp. 4081-4085

Hassani, H. et al (2014), *A dosimetric study of small photon fields using polymer gel and Gafchromic EBT films,* Medical Dosimetry, Vol. 39, pp. 102-107

Hayton, A. (2011), *Investigation of the MOSkin detectors for use in dosimetry of a HDR Brachytherapy source,* School of Applied Science, RMIT University

Heydarian, M. et al (1996), *A comparison of dosimetry techniques in stereotactic radiosurgery*, Physics in Medicine and Biology, Vol. 41, pp. 93-109

Holmes-Siedle, A.G., (1974), *The space charge dosimeter, general principles of a new method of radiation dosimetry*, Nuclear Instrumentation and Methods, Vol. 121, pp. 169-172

Hsu, S.M. et al (2011), *Dose measurements for gamma knife with radiophotoluminescent glass dosemeter and radiochromic film,* Radiation Protection Dosimetry, Vol. 146, pp. 256-259

IAEA (2000), *Absorbed dose determination in external beam radiotherapy*, Technical report series No. 398, IAEA, Vienna, Austria

IBA (2011), *Detectors for relative and absolute dosimetry,* IBA, Supplier Specifications Pamphlet, Schwarzenbruck, Germany

ICRU, (1999), *Prescribing, recording and reporting photon beam therapy*, Report 62, Journal of the ICRU, Vol.4

International Specialty Products (2011), *Gafchromic EBT3 film*, Supplier Specifications Pamphlet, International Specialty Products, New Jersey, USA

Jaffray, D.A. et al (1993), *X-ray sources of medical linear accelerators: focal and extra focal radiation*, Medical Physics, Vol.20, pp. 1417-1427

Kelashvili, Gocha. et al (2012), *Dosimetric characteristics of the small diameter BrainLab™ cones used for stereotactic radiosurgery,* Journal of Applied Clinical Medical Physics, Vol. 13, http://www.jacmp.org/index.php/jacmp/article/view/3610/2399, accessed January 2014.

Khan, F.M, *The Physics of Radiation Therapy*, Third Ed., Lippincott Williams and Wilkins, Philadelphia, USA

Knoll, G.F (2000), *Radiation detection and measurement*, Third Ed., John Wiley and Sons, New Jersey, USA

Kron, T. et al (2002), *Measurements in Radiotherapy Beams using n-line MOSFET detectors*, Radiation Protection Dosimetry, Vol. 101, pp. 445-448

Kwan, I. S. (2009), *Characterization of the performance of the new MOSkin dosimeter as a quality assurance tool for pulsed dose-rate (PDR) prostate brachytherapy, and the effect of rectal heterogeneity on the dose delivered to the rectal wall,* PhD Thesis, School of Engineering Physics, University of Wollongong

Larson, D.A et al (1994), *Consensus Statement on stereotactic Radiosurgery quality improvement,* Report of the ASTRO and AANS task force on stereotactic radiosurgery, International Journal of Radiation Oncology, Biology and Physics, Vol. 28, pp. 527 -530

Laub, W.U and Wong, T. (2003), *The volume effect of detectors in the dosimetry of small fields used in IMRT*, Medical Physics, Vol. 30, pp. 341-347

Leksell, L. (1983), *Stereotactic radiosurgery*, Journal of Neurology, Neurosurgery and Psychiatry, Vol. 46, pp. 797-803

Lewis, D. F (2012), *Practical Guidance for using Radiochromic Film*, Ashland Specialty Ingredients, http://www.filmqapro.com/Documents/Lewis_Radiochromic_Film_20120209.pdf, accessed August 2014

Lightstone, A. W. et al(2005), *Intracranial stereotactic positioning systems*, Report of the AAPM radiation therapy committee task group 68, Medical Physics, Vol. 32, pp. 2380 - 2398

Low, D.A. et al (2003), *Ionisation chamber volume averaging effects in dynamic intensity modulated radiation therapy beams*, Medical Physics, Vol. 30, pp. 1706-1711

Martens, C. et al. (2000), *The value of the PinPoint ion chamber for characterisation of small field segments used in Intensity Modulated radiotherapy*, Physics in Medicine and Biology, Vol. 45, pp. 2519-2530

McKerracher, C. et al (1999), *Assessment of new small field detectors against standard field detectors for practical stereotactic beam data acquisition*, Physics in Medicine and Biology, Vol. 44, pp. 2143-2160

Metcalfe, P., Kron, T. And Hoban, P. (2003), *The Physics of Radiotherapy X-rays and Electrons*, Medical Physics Publishing, Wisconsin, USA

Morales, J. E. et al (2014), *A comparison of surface doses for very small field x-ray beams: Monte Carlo calculations and Radiochromic film measurements*, Australasian College of Physical Scientists and Engineers in Medicine, Vol. 37, pp 303-309

Morin, J. et al (2013), *A Comparative study of small field total scatter factors and dose profiles using plastic scintillation detectors and other stereotactic dosimeters: The case of the CyberKnife,* Medical Physics, Vol. 40, pp. 011719-1 – 011719-11

Morton, J. (2006), *Clinical Implementation of MOSFETS for Entrance Dose In-Vivo Dosimetry with High Energy Photons for External Beam Radiation Therapy*, School of Chemistry and Physics, University of Adelaide

Nahum, A. E., (1996) *Perturbation effects in dosimetry: Part I. Kilovoltage x-rays and electrons*, Physics in Medicine and Biology, Vol. 41, pp. 1531-1580

Naidoo, P. (Unknown date), M*icro-multileaf Collimator vs Cones for Stereotactic Radiosurgery*, NetCare Parklands Hospital. [Presentation]

Niroomand-Rad, A et al (1998), *Radiochromic Film Dosimetry*, Report of the AAPM radiation therapy committee task group 55, Report No. 63, Medical Physics, Vol. 25

Otto, K (2008), *Volumetric modulated arc therapy: IMRT in a single gantry arc*, Medical Physics, Vol. 35, pp. 310-317

Pappas et al (2008), *Small SRS photon field profile dosimetry performed using a PinPOint air ionisation chamber, a diamond detector, a novel silicon-diode array (DOSI), and polymer gel dosimetry*. *Analysis and intercomparison,* Medical Physicsw, Vol. 35, pp. 4640-4648

Peet, D.J. and Pryor, M. D. (1999), *Evaluation of a MOSFET radiation sensor for the measurement of entrance surface dose in diagnostic radiology*, The British Journal of Radiology, Vol. 72, pp. 562-568

Pogorsak, E.B. (2005), *Radiation Oncology Physics: A handbook for teachers and students*, IAEA, Vienna, Austria

Potters, L et al (2006), *Practice Guidelines for the Performance of Stereotactic Body Radiation Therapy*, Report of the ASTRO and ACR, International Journal of Oncology, Biology and Physics, Vol. 60, pp. 1026 - 1032

PTW Freiburg (2013), *Radiation Therapy: Small field dosimetry*, Supplier application guide, Germany

Qi, Z. Y. (2010), *Mosfet dosimetry in HDR brachytherapy and IMRT for nasopharangeal carcinoma*, Doctor of Philosophy Thesis, Engineering physics, University of Wollongong

Ralston, A. et al (2012), *Small field diode correction factors derived using an air core fibre optic scintillation dosimeter and EBT2 film*, Physics in Medicine and Biology, Vol. 57, pp. 2587-2602

Ramani, R., Russel, S. and O'Brien, P. (1997), *Clinical dosimetry using MOSFETs*, International Journal of Radiation Oncology, Biology and Physics, Vol.37, pp. 959-964

Ramaseshan, R. et al (2004), *Performance characteristics of a microMOSFET as an in vivo dosimeter in radiation therapy*, Physics in Medicine and Biology, Vol. 49, pp. 4031-4048

RANZCR, *What is radiation Therapy*, http://www.ranzcr.edu.au/radiation-oncology/what-is-radiation-therapy, unknown date, accessed 10/2014.

Reinhardt, S. et al (2012), *Comparison of Gafchromic EBT2 and EBT 3 films for clinical photon and proton beams*, Medical Physics, Vol. 39

Richley, L., et al (2010), *Evaluation and optimisation of the new EBT2 radiochromic film dosimetry system for patient dose verification in radiotherapy*, Physics in Medicine and Biology, Vol. 55, pp. 2601-2617

Rosenfeld, A.B. (2011), *Advanced Semiconductor dosimetry in radiation therapy*, In A. Rosenfeld (Eds.), Concepts and trends in medical radiation dosimetry, pp. 48-74, Melville, USA, American Institute of Physics

Rosenfeld. A. B. (2002), *MOSFET dosimetry on modern radiation oncology modalities*, Radiation Protection Dosimetry, Vol. 101, pp. 393-398

Rosenfeld. A. B., et al (2001), *Feasibility study of online high-spatial-resolution MOSFET dosimetry in static and pulsed x-ray radiation fields*, IEEE Transactions on Nuclear Science, pp. 2061-2068

Rowshanfarzad. P, et al (2011), *Isocentre verification for linac-based stereotactic radiation therapy: review of principles and techniques*, Journal of applied clinical medical physics, Vol. 12, pp. 185-195

Ruud, G.J., et al. (2009), *Stereotactic Radiotherapy of Intracranial Tumours: A Comparison of Intensity Modulated Radiotherapy and Dynamic Conformal Arc*, International Journal of Radiation Oncology, Biology and Physics, Vol. 74, pp. 1018-1026

Schell, M. C. et al (1995), *Stereotactic Radiosurgery, Report of the AAPM radiation therapy committee task group 42*, Report No. 54, AAPM

Schofield, D., Ramsey, G. (2012), *The Safe Implementation of Stereotactic Radiosurgery in the Community Hospital Setting*, American Association of Medical Dosimetrists, [Presentation]

Scott. A.J.D. et al (2012), *Characterising the influence of detector density on dosimeter response in non-equilibrium small photon fields*, Physics in Medicine and Biology, Vol. 57, pp. 4461-4476

Selvam, T.P and Keshavkumar, B. (2010), *Monte Carlo investigation of energy response of various detector materials in I-125 and Yb-169 brachytherapy dosimetry*, Journal of Applied Clinical Medical Physics, Vol. 11, http://www.jacmp.org/index.php/jacmp/article/view/3282/2024, accessed 27/03/15.

Seung, S. K et al (2013), *Practice Guidelines for the Performance of Stereotactic Radiosurgery*, Report of the ASTRO and ACR, American Journal of Clinical Oncology, Vol. 36, pp. 310 - 315

Seutjens, J. (2011), *Small field dosimetry for IMRT and Radiosurgery*, [Presentation], SEAAPM

Shaw, E et al (1993), *Radiation Therapy Oncology Group: radiosurgery quality assurance guidelines*, International Journal of Radiation Oncology, Biology and Physics, Vol. 1, pp. 1231 - 1239

Siemens healthcare (2011), *Innovative solutions for radiation therapy: Siemens at ESTRO 2011*, http://www.siemens.com/press/en/pressrelease/?press=/en/pressrelease/2011/imaging_therapy/him201105028.htm, accessed Feb 2014.

Tavernier, S. et al. (2006), *NATO Advanced Research Workshop on Radiation Detectors for Medical Applications*, Radiation Springer, Netherlands

Taylor, M.L., Kron, T., Franich, R.D. (2011), *A contemporary review of stereotactic radiotherapy: Inherent dosimetric complexities and the potential for detriment*, Acta Oncologica, Vol. 50, pp. 483-508

Taylor. M. L (2010), *On the characterisation of stereotactic radiation therapy fields*, PhD Thesis, School of Applied Sciences, RMIT University

Teh, B.S. et al (1999), *Intensity modulated radiation therapy (IMRT): A promising technology in radiation oncology*, The Oncologist, Vol. 4, pp. 433-442

Thomson-Nielsen (Unknown date), *Introduction to the MOSFET Dosimeter*, Technical Note 4, Best Medical, Canada, http://www.mosfet.ca/global/pdf/technotes/te_4.pdf, accessed Feb 2014

Tyler, M. et a., (2013), *Characterisation of small field stereotactic radiosurgery beams with modern detectors*, Physics in medicine and biology, Vol. 58, pp. 7595-7608

Web, S. Et al (2002), *Intensity Modulated Radiation Therapy*, second reprint, Institute of Physics Publishing, London, UK, pp. 1-18

Westermark, M. et al (2000), *Comparative dosimetry in narrow high energy photon beams*, Physics in medicine and Biology, Vol. 45, pp. 685-702

Wong, J.H.D., et al (2011), *The use of a silicon strip detector dose magnifying glass in stereotactic radiotherapy QA and dosimetry*, Medical Physics, Vol. 38, pp. 1226-1238

Wuerfel, J. U. (2013), *Dose Measurements in Small Fields*, Medical Physics International, Vol. 1, pp. 81-90

Zahra, D. (2009), *MOSFET dosimetry: MOSkin dosimetric characteristics in a 6 MV x-ray beam*, PhD Thesis, School of Engineering Physics, University of Wollongong